

Nanoparticles Modified Electrodes: Synthesis, Modification, and Characterization—A Review

Temitayo O. Falola

Department of Chemistry, Illinois State University, Normal, Illinois, USA

Email: tofalol1@ilstu.edu, falolatemitayo09@gmail.com

How to cite this paper: Falola, T.O. (2022) Nanoparticles Modified Electrodes: Synthesis, Modification, and Characterization—A Review. *World Journal of Nano Science and Engineering*, 12, 29-62.
<https://doi.org/10.4236/wjnse.2022.123003>

Received: December 24, 2021

Accepted: September 27, 2022

Published: September 30, 2022

Copyright © 2022 by author(s) and Scientific Research Publishing Inc.

This work is licensed under the Creative Commons Attribution International License (CC BY 4.0).

<http://creativecommons.org/licenses/by/4.0/>



Open Access

Abstract

Nanoparticles offer unique features such as a larger surface area and enhanced electrochemical performance compared to their contemporary matters. These properties make them suitable to be considered in bridging the lacunae associated with the use of bare electrodes in electrochemical sensors. Nanomaterials enhance the redox reversibility on the electrodes' surfaces, hence, improving the reproducibility, sensitivity, and limit of detection of the electrodes/sensors. Their methods of synthesis (top-to-bottom and bottom-to-top) are tailored toward manipulating their sizes, shapes, and preventing their agglomeration. This review paper provides a synopsis on research done in synthesizing nanoparticles, modifying electrodes, and pinpointing the improved performances of the modified electrodes via known characteristic techniques, namely: cyclic voltammetry, differential pulse voltammetry, and electrochemical impedance spectroscopy. In addition, a perspective is given in terms of increasing the lifespan of the working electrodes and the need for non-faradaic sensors.

Keywords

Nanoparticles, Turkevich Method, Modification, Characterization, Limit of Detection, Redox Reversibility, Electrochemical Properties

1. Introduction

Nanoparticles are substances with sizes in the order of 10^{-9} m. This small magnitude is the major factor for their enhanced reactivities, better physical and chemical properties over their corresponding native substances. Nanomaterials have applications in numerous areas, such as drug delivery (to maximize drug efficacy and minimize cytotoxicity); reinforcing the mechanical properties of bioplastic films [1] and composite materials; improving the electrochemical properties of sensors semiconductors, and so on. The large surface-to-volume

ratio of these particles can allow better ligand-to-site binding; hence, decreasing dosage [2], increasing oral bioavailability, the latter of which improves patient compliance. They also play important roles in catalysis where catalytic activity is increased due to the particles' high surface area. The catalytic reactions are done under mild conditions to ensure the stability of the particles against decomposition [3]. Metallic nanoparticles such as palladium nanoparticles catalyze C-C cross-coupling reactions as in Heck coupling, Negishi, and Suzuki coupling reactions. Nanostructures have shorter bi-continuous ions which give better battery performance when used as battery electrodes [4]. Tailored nanoparticles are major backbones of the recent generation solar cells [5]. Nanotechnology is employed to mitigate catalyst poison in fuel cells such as hydrogen fuel cells where separation of the atoms' electrons and protons is possible in the presence of a nanosized palladium catalyst, the catalyst of which is sensitive to carbon (II) oxide [6]. Nanomaterials are also employed in electronics [7], preparation of asphalt, environmental remediation, high energy density batteries, preparation of sunscreen [8], medical implants, and so on. Examples of materials used for the applications mentioned above are nanosilver, nanoparticles silica [9], carbon nanotubes, nanocrystalline nickel-metal hydrides, zinc oxide nanorod, and nanoceramics, respectively.

This paper focuses on the synthetic routes of nanoparticles used in modifying working electrodes towards electrochemical sensing, how the nanoparticles are deposited on the electrodes' surfaces, and the methods explored in their characterization. Nanoparticles' synthesis can be carried out via several methods, such as physical, chemical, and biosynthetic approaches. The first two methods (also called top-to-bottom techniques) give uniform-sized highly stable nanoparticles with the release of hazardous materials into the ecosystem. On the other hand, the biosynthetic (bottom-to-top) routes utilize eco-friendly reducing agents and stabilizing agents including either fungi, yeasts, bacteria, and plants or their active constituents.

Sensors use working electrodes as their transducer element. They couple a chemically sensitive layer to an electrochemical transducer giving a real-time translation to a piece of information about the composition of a particular system [10]. They are commonly used for detecting trace levels (in part per billion) of toxic gases such as carbon (II) oxide, hydrogen sulfide, carbon (IV) oxide (greenhouse gas), and chlorine. Sensors are modeled to consist of three electrodes: working electrode, reference electrode, and counter electrode. Selectivity can be improved by tuning the potential difference between the counter electrode and the working electrode. The redox reaction between the analyte and the membrane of the electrode releases a certain amount of ampere which is proportional to the concentration of the gas of interest [11]. Zhan *et al.* argued that electrochemical sensing offers superiority over instrumental techniques due to its low cost, easy operation, simple measurement system, high sensitivity, and real-time analysis for on-site detection [12].

Nanoparticles are now used on the working electrodes to increase the surface area for the chemical reactions; hence, reducing noise level and enhancing detection bands, even for trace analytes [13]. Gold nanoparticles (AuNPs) have shown potential in serving as internal reference probes. For example, Ozsoz *et al.* designed a Factor V Leiden mutation determining electrochemical genosensors, measuring the signal by using AuNPs oxidation signal [14]. Similarly, Kermal *et al.* reported an electrochemical-based method for detecting DNA hybridization based on changes in AuNPs oxidation signal [15]. AuNPs allow less intrusive imaging techniques due to their optical qualities [16]. With these optical properties, AuNPs play an important role in biosensors [17]. Eduart Gutierrez Pineda *et al.* designed an AuNPs-coated polypyrrole films (AuNPs/Ppy) composite electrode that provides low ohmic-drop pathways due to the porous structure of the film, whilst the gold nanoparticles increase the metallic surface redox reaction's rate constant [18]. In addition, Au/Ppy nano and microstructure electrodes provide good sensitivity, conductivity, and catalytic properties [19]. AuNPs maintain well-layered distribution on the surface of electrodes. Electrodeposition of Au from its salts is a common method for depositing AuNPs on electrodes among other methods documented by researchers. Fan *et al.* designed an electrochemical sensor with a silica nanoparticle modified working electrode for quantifying prostate-specific antigens [20]. Zhou *et al.* documented a single probe dual-signal sensor coated with mesoporous SiO₂ nanoparticles coupled with silver nanoparticles (AgNPs) [21]. The high dispersity of Ag clusters makes it easier to be coupled with biomolecules [22].

Also, Tortolini *et al.* modified screen-printed electrodes (SPEs) with nanoceria for detecting total antioxidant capacity e.g. gallic acid, ascorbic acid, caffeic acid, dimethyl sulfoxide, in wine samples [23]. In the same vein, Abdel-Raouf *et al.* developed an electrochemical sensor that can detect oxymetazoline hydrochloride via the modification of SPEs with nanoceria [24]. This sensor utilizes paraffin oil and nanoceria to increase electrical sensitivity. Noteworthy, the sensor performed well for five straight months, showing stable reproducibility and significant linear response.

Likewise, pristine graphene shows high sensitivity and high signal-to-noise ratio due to the high electron mobility, good conductivity, high surface area, and negligible crystal defects of the 2-dimensional structure of graphene nanosheets [25]. Arsat *et al.* and Hafiz *et al.* stated the efficacy of pristine graphene in the detection of H₂ and CO₂ [26] [27]. Chatterjee *et al.* state that surface functionalization of an electrode by doping with these nanoparticles improves its sensitivity [28]. Zhu *et al.* detected bisphenol A, an endocrine-disrupting chemical in food and beverage containers using glassy carbon electrode (GCE) coated with flower-like bimetallic Pt/Pd nanoparticles, which was synthesized via microwave-assisted hydrothermal method [29]. The electrochemical detection is linear, with analyte concentrations spanning from 0.75 μ M to 600 μ M, and a detection limit of 132 nM. Sharma *et al.* buttress that the synergistic effects created

by two noble metals such as Pt/Pd above greatly enhance the performance of the electrode [30]. These modifications are often investigated using both voltammetry (cyclic and/or differential pulse) and electrochemical impedance spectroscopy.

2. Synthesis of Nanoparticles Used in the Modification of Electrodes

The ability of nanoparticles to interact with light rays causes them to be highly sought after in modern science. Talking about the properties of nanoparticles, they undergo a phenomenon known as surface plasmon resonance (SPR). This phenomenon occurs when a rapid oscillation of the bulk of electrons on the surface of a light bombarded metal creates an electromagnetic response. Also, nanoparticles have a large surface area which makes them react to external stimuli at a breakneck speed. Nanoparticles' methods of synthesis (Figure 1) are majorly classified into two: bottom-to-top and top-to-bottom approaches. Assembling of atoms/molecules to produce different forms of NPs describes the bottom-down approach, while the mechanical breakdown of the large metal structure in the size distribution and morphologies controllable energy-demanding approach called top-to-bottom.

2.1. Gold Nanoparticles

In recent years, AuNPs have been in high demand due to their biocompatibility, inertness, and high electrical conductivity. To manipulate their properties to fit specific purposes, different factors such as reaction conditions (temperature, pH, and concentration) [31], dispersed medium *i.e.* solvents, stabilizing agents [32], incorporation of different reactants [33]; have been altered in several studies. The most promising method "Turkevich" has been utilized due to its simplicity. In this process, nano-sized particles are generated from the reaction between chloroauric acid and a small amount of mild reducing agents such as sodium citrate, ascorbic, and tannic acid, taking place in an aqueous medium. The particles

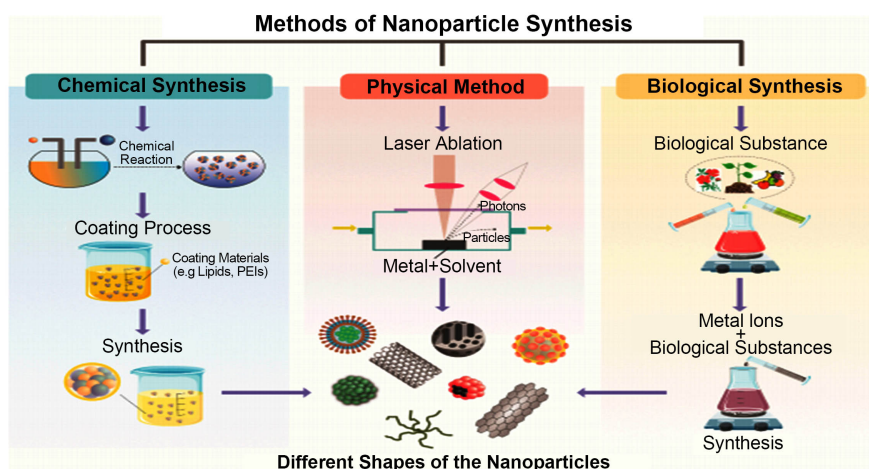


Figure 1. Chart showing the methods of nanoparticles synthesis [32].

might be nanorods or nanocages/cubes. It is important to highlight the quintessential role of solvent in this synthesis. The interaction between the solvent and the capping/reducing agent influences the size and surface functionalization of the final product [34]. In the presence of a highly polar solvent, the nanoparticles absorb a greater amount of charged ions leading to an increase in point zero charges (zeta potential) because a strong electrical double layer forms around the nanoparticles [35].

Additionally, the increase in zeta potential increases repulsion between the nanosized particles; hence, preventing agglomeration. Hussain *et al.* synthesized GNPs via the chemical reduction method (CRM), which they refer to as a modified version of Turkevich methodology [36]. Usually, CRM depends on varying factors such as the reaction time, stabilizer concentration, precursor concentration, among others [37]. Here, they injected 5 ml of HAuCl_4 solution into a solution of L-ascorbic acid in the presence of polyvinyl pyrrolidone (PVP) as a stabilizer which protected the nanoparticles from aggregating, while the former was a reducing agent. The initial concentrations of the two main reactants were set at a ratio of 1:10, and the medium was a mixture of ethanol and water which was varied to study the efficacy of the polarity index of the reaction's dispersed medium. They suggest that the relationship between the index and the size of the nanoparticles is inverse. So, the size of AuNPs can be manipulated by adjusting the percentage volume of the organic component of the reaction medium. Hedkvistv and Toprak reported the synthesis of nanospheres gold particles using the Brust two-phase method, where the capping agent (which regulates particle growth and prevents agglomeration) and the primary reductant was the thiol-ligand, and NaBH_4 served as the second reducing agent [38]. The idea proposed is that oil-soluble thiol helps to transfer the HAuCl_4 from water to oil in a mixed water-oil dispersed media. This allows effective control of particle size by varying the ratio of NaBH_4 and HAuCl_4 . According to Li and Lou, AuNPs obtained from the Brust-Schiffrin method described above do have high stability due to the strong interaction between Au and thiol and can be easily functionalized [39]. Driskell *et al.* synthesized 60 nm gold particles via the modified thermal reduction method. In this work, they stirred for 15 minutes 2 mL of 1 wt% $\text{HAuCl}_4 \cdot 3\text{H}_2\text{O}$ solution, and heated to boiling; then, 1.5 mL trisodium citrate was added leading to the formation of spherical AuNPs [40]. Also, AuNPs have been prepared by using UV-irradiation, thermal reduction of HAuCl_4 in the dense phase of the block copolymer, and photoreduction [41]. More so, Han's research group produced Au nanorods (AuNRs) via ultrasound irradiation of HAuCl_4 solution which contained α -D-glucose as a directing agent [42].

The green method of synthesis has seen scientists utilize plants, fungi, enzymes, algae, and biopolymers to produce safer AuNPs for use in biomedicine [43]. Gold nanorods (AuNRs) were synthesized with high yield and good dispersity by a seed-growth method developed by Murphy, Gearheart, and Jana [44]. Likewise, Paul *et al.* synthesized AuNPs via the tip-selective growth method, the product of which finds applicability in optical waveguides [45].

2.2. Carbon Nanotube (CNTs)

CNTs are tube-like molecular structured allotropes of carbon. They can exist as single-walled CNTs (SWCNTs) or multi-walled CNTs (MWNTs). SWCNTs are covalently linked carbon atoms that form a one-dimensional structure of about 1 nm in diameter and length that is several thousand nanometers. They are semi-conducting material with intrinsic photoluminescence properties such as the ability to penetrate deep tissue beyond 1 mm, hence, their use for near-infra-red (NIR) photoluminescence imaging [46]. MWNTs are made of several cylindrical-shaped concentric tubes. Unlike SWNTs, their diameters may be as much as about 30 nm, while the length is 100 times the diameter. They are entangled and straight, contributing to their vast performance and applications. They are known to increase the tensile strength and the young modulus when incorporated into polymeric materials. They can be functionalized to enhance the performance, strength, and dispersity of composites [47].

Both SWCNTs and MWCNTs possess a large surface-to-volume ratio, magnificent mechanical strength, and excellent electrical conductivity due to the presence of sp^2 hybridization between adjacent carbon atoms; hence, they are used as ingredients for electrode structure [48]. Thermal chemical vapor deposition is one of the methods for synthesizing CNTs. Here, hydrocarbon gas is pumped into a quartz tube (wherein is placed a crucible containing silica or zeolite-substrate) filled with a noble gas such as helium. The quartz tube is heated in a furnace as the hydrocarbon undergoes pyrolysis into carbon atom vapor. The carbon atoms bind on the substrate and grow into a mass of MWCNTs held together by van der Waal's force of attraction [49]. Another method uses an electric arc discharge. In this method, two pure graphite electrodes are kept 1 mm apart and supplied with 500 torrs of helium gas inside a quartz chamber. The energy produced in the electric arc when the two electrodes strike each other is transferred to the positive electrode which oxidizes the carbon atoms to produce gaseous phase carbon ions. These ions get reduced at the cathode and grow into CNTs. The increase in the mass of CNTs decreases the size of the anode. If the noble gas pressure is maintained, uniform deposition on the cathode can be achieved [50].

The last method to be mentioned in CNTs synthesis is the physical vapor deposition, also known as the laser ablation method. Here, graphite is centralized in a quartz chamber filled with noble gas at 1200°C ; then, a laser is used to vaporize the graphite, and the resultant gaseous phase carbon atoms are cooled and deposited on the copper collector. When a continuous laser beam is used, continuous vaporization of the carbon atoms is achieved, whilst pulsed laser beam provides monitoring of the CNTs produced. To synthesize SWCNTs, nanoparticles of Fe or Ni can be used as the substrate coated on the anode, and in place of the water-cooled copper collector, in each case [51].

2.3. Nanoceria

Several methods have been adopted to synthesize nanoceria in different sizes,

shapes, distribution, and agglomeration. Compounds of ceria such as cerium nitrate, cerium chloride, cerium sulfate have been converted to cerium oxide for the synthesis of its nanosized particles [52]. Nanoceria has attractive properties such as biocompatibility, oxygen transferability, and good electrical conductivity which encourage its use in developing electrochemical sensors, wherein it increases the sensitivity, stability, and response time of the sensors. A Few of the methods that have been used to synthesize nanoceria will be covered here. Nanocrystals of ceria can be formed at room temperature under alkaline conditions, using cerium nitrate hexahydrate as the precursors [53]. In this case, poly(ethylene)imine can serve as a complexing agent and a potassium salt of carboxymethylated poly(ethylene)imine dispersing agent. In another case, Junais and Govindaraj developed a precipitation method using polyvinyl pyrrolidone (PVP), polyvinyl alcohol (PVA), and ammonium hydroxide, as a dispersing agent, complexing agent, an alkaline medium, respectively [54].

When it comes to being able to control the size and shape of the synthesized nanoceria, the hydrothermal method is perhaps the best to consider as it allows such variations by controlling parameters such as pH, reaction time, solute concentration, temperature, and solvent type. Stelmachowski *et al.* synthesized ceria nanorods from cerium hexahydrate and urea [55], while Fisher *et al.* and Jayakumar *et al.* utilized cerium nitrate as the precursor to synthesize shape-specific nanoceria controlled by molarity of alkaline, pH, and reaction time [56] [57]. Also, Khairy *et al.* adjusted the pH of aqueous cerium (III) chloride using aqueous ammonia to give a white precipitate of 40 nm nanoceria [58]. Another method is the solvothermal method in which a liquid or supercritical medium is employed at high temperature. Pang *et al.* prepared nanoceria with cerium (III) nitrate using water and alcohol as liquid media. Hydrogen peroxide and aqueous ammonia were added, followed by mixing the precipitates formed with alcohol before heating in an autoclave [59]. Alternatively, this method can be carried out by substituting in deep eutectic solvent (an ionic liquid) as the liquid medium, which depresses the glass transition temperature.

Recently, the utility of plants, fungus, biopolymers as green synthesis methods has gained ground. This eco-friendly method utilizes plant extracts as both stabilizing and capping agents. Sharmila *et al.* reported a procedure in which CeCl_3 heptahydrate was added to a hydro-extract of *Aquilegia pubiflora* at a warm temperature, dried, and calcined at 500°C [60]. In this case, the extracts of the plant: flavonoids (vitexin and isovitexin), hydroxycinnamic, and ferulic acid serve as reducing and capping agents. The particle size was 28 nm. In another work, aqueous cerium nitrate was mixed with a solution of chitosan, and aqueous ammonium hydroxide was added till a pH of 10 was reached. Then, the solution was stirred at 70°C until gel-like nanoparticles were obtained [61].

2.4. Graphene

The carbon atoms of graphene have a honeycomb-like sp^2 hybridization. Its

structure consists of three in-plane σ -bonds which hold the atoms together, and out-of-plane π -bonds with unpaired electrons with high mobility [62]. The latter forms π and π^* bonds, allow electronic transitions; hence, making graphene a good conductor of electricity at room temperature [63]. Its electrical conductivity and surface area are remarkably $100 \text{ S}\cdot\text{cm}^{-1}$ and $2600 \text{ m}^2\cdot\text{g}^{-1}$, respectively. Somani *et al.* applied a chemical vapor deposition method to synthesize graphene nanosheets using camphor pyrolysis at about 850°C with Ni substrate and Ar as carrier gas [64]. They reported a transmission electron microscope (TEM) imaging that reveals a nanosheet in size of approximately 0.34 nm. Sun *et al.* grew a monolayer pristine graphene film from poly (methylmethacrylate), using copper as substrate at 800°C resulting in a material with 0.7 nm thickness as measured by atomic force microscopy (AFM) [65].

In another study, researchers synthesized large-scale graphene from the first three members of primary alcohol as precursors on copper foil [66]. At the growth temperature of 850°C , Cu film was then exposed to the alcohol vapor for 5 minutes. The precursors gave monolayer sheets of graphene with Raman spectra confirming that the synthesized material is of high quality with no oxidation effect.

2.5. Platinum Nanoparticles (PtNPs)

PtNPs synthesis is akin to that of AuNPs in some ways. Both physical, chemical, and biological methods have been adopted to synthesize platinum nanoparticles. Physical methods involve the use of radiation, heat energy, mechanical pressure, or electrical energy to generate nanosized particles. While these methods are advantageous due to their high speed, uniform size, and shape formation, their demerits are not limited to high cost, exposure to radiation, high energy, less thermal instability, difficult shape and size tuneability. This method is known to change the morphology and physicochemical properties of the nanoparticles. Techniques under these categories are solvothermal process, vapor deposition, inert gas condensation (IGC), milling, and flame pyrolysis [67], to mention but five. In the milling process, the particle size is reduced and homogenized. The solvothermal process increases the solubility of the reactants at a low temperature under pressure. IGC is a very efficient method for synthesizing good quality PtNPs. It involves the evaporation of metals in inert gas-filled vacuum chambers at about 100 Pa. similar to AuNPs synthesis, an elastic collision occurs between the gas atoms, whilst the evaporated metal atoms condense to give crystal as a result of a drop in their kinetic energy [68].

The chemical method involves the use of water-soluble cations as raw materials to initiate their reduction to metal monomers. Several chemical methods that have been employed are wet chemical reduction, microemulsion, electrochemical process, chemical reduction, co-precipitation, among others. Wet chemical reduction mainly controls particle sizes; chemical reduction is used for producing colloidal NPs. The shape and size of the synthesized PtNPs depend on

the reducing agent [69], reaction temperature [70], and concentration of the platinum compound. The advantages of the chemical method are easy functionality, high yield, the thermal stability of the product, and reduced dispersity, but its disadvantages are low purity and the use of toxic chemicals.

Alternatively, researchers have reported the eco-friendly synthesis of PtNPs using biological precursors. Majorly, this process involves uptake and deposition. Riddin *et al.* synthesized geometric PtNPs using cell-soluble protein extracts from sulfate-reducing bacteria [71] such as *Desulfovibrio desulfuricans* [72] and *Acinetobacter calcoaceticus* [73]. These micro-organisms reduce Pt^{4+} into 2 - 3.3 nm cuboidal structured PtNPs at pH 7.0 and 30°C. Shen *et al.* produced PtNPs from *Anacardium occidentale* leaf extracts at pH 6 to 9 [74]. The transmission electron microscope revealed the formation of crystalline rod-shaped NPs. Dauthal *et al.* fabricated spherical 16 to 23 nm PtNPs from *Punica granatum* peel extract. FTIR spectrum shows a shift in peak from 3439 cm^{-1} to 3424 cm^{-1} , indicating the presence of a phenolic group was in the extract, and that was responsible for reducing and stabilizing NPs [75].

3. Modification of Electrodes with Nanoparticles

Limitations surround the use of electrochemical sensors due to their poor reproducibility, poor detection limit, and non-reliability which often come from variations in electrodes' morphology and area, density, nontarget-induced reagent degradation, and complex detection matrices [76]. However, nanoparticles have bridged these lacunae in that they offer unique electrochemical properties compared to their corresponding atoms when coated on the electrodes' surfaces. For instance, electrochemical detection, dual excitation, or emission dyes (methylene blue and ferrocene) which work for luminescence, ratiometric methods are hard to mobilize on sensors' electrodes surfaces where high stability is expected. The reason is not far-fetched: they must be labeled on DNA chains. This DNA-assisted ratiometric sensing greatly increases the complexity of the instrument operation [77]. Sequel to these, efforts in developing working electrodes that are less complicated and allow easier electrochemical detection are on their geometric progression. Researchers have modified electrodes with nanoparticles to overcome the less superior features of bare electrodes.

Lei *et al.* reported the use of a GCE coated with poly (2-amino terephthalic acid), (ATA), film doped with CNTs, and mercaptosuccinic acid (MSA-CNTs-ATA/GCE) for the electrochemical detection of Cd^{+2} , Hg^{+2} , Pb^{+2} , and Zn^{+2} [78]. Lei and co-workers used bismuth (III) in anodic stripping voltammetry as both enhancer and internal reference giving the electrode a better sensitivity and excellent voltammetric responses to the abovementioned ions. They initially polished the bare GCE with alumina slurries and ultrasonicated with dilute HNO_3 , ethanol, and water. The GCE was dipped in 10 mL of phosphate buffer solution (PBS) containing 2.0 $mmol \cdot L^{-1}$ ATA, 0.20 $mg \cdot mL^{-1}$ CNTs, and 5 mM H_2SO_4 ;

scanned at $10 \text{ mV}\cdot\text{S}^{-1}$ from 0.4 to 1.2 V to polymerize the CNT-doped ATA film on the electrode surface. Then, in addition to being washed with ethanol and dried with a stream of N_2 , the CNT-ATA/GCE was again scanned for two cycles (0.2 - 0.8 V, $20 \text{ mV}\cdot\text{S}^{-1}$) in 5 mM MSA + $0.1 \text{ mol}/\text{dm}^3 \text{ H}_2\text{SO}_4$ to give the MSA-CNTs-ATA/GCE. The bismuth film's current peak served as the reference electrode which gives the ratiometric measurement, while the ratio of the stripping current peak to that of Bi^{+3} corresponds to the signal indicator [79]. The modified electrode shows improved performance. The authors stated that the electrochemical strategy offers in addition to high sensitivity, an easier experimental operation, reliability, and possibility for simultaneous determination of heavy metal ions and perform immunoassays.

Nanoceria is another nanoparticle been used as a transducer due to its high sensitivity [80]. Nanoceria gives sensors' electrodes better reactivity due to the multiple oxygen vacancy defects in its crystal structure, and high ionic conductivity. These provide nanoceria with unique features such as increased catalytic activity, surface reactivity, ability to transfer oxygen, switchable redox reactivity from Ce^{3+} to Ce^{4+} , making it function as a transducer in electrochemical sensing. In addition, nanoceria can be employed in detecting analytes in biological matrices as it has good biocompatibility, high zeta potential, and adsorption capacity, and is non-toxicity [81]. Jiang *et al.* modified the surface of GCE by dropping and dispersing CeO_2 and adding chitosan to stabilize the CeO_2 nanocrystalline [82]. The modified electrode was then immersed in tetra chloroauric acid (HAuCl_4) solution. Then, gold was deposited on the electrode surface at constant potential over time. The sensor showed reproducibility, stability, and selectivity with a detection limit of $2.86 \times 10^{-3} \text{ mM}$. Meng *et al.* attached a chitosan/cerium oxide composite on the GCE surface to detect glucose in the range between 2.0 μM and 1.8 mM, and the detection limit was 0.8 μM [82]. Moreso, the improved electrochemical response given by $\text{CeO}_2/\text{Ni}(\text{OH})_2$ nanocomposite on carbon plate electrode has been attributed to the synergy between CeO_2 and $\text{Ni}(\text{OH})_2$ [83]. This sensor can be utilized for H_2O_2 quantification towards diagnosing pathological conditions such as infections and inflammation [84]. Iranmanesh *et al.* reported the detection of dopamine, uric acid, ascorbic acid, and acetaminophen by modifying the surface of GCE with CeO_2 [85]. The detection limits were 3.1 nM, 2.4 nM, 2.6 nM, and 4.4 nM, respectively.

Modification of GCE with PtNPs has also been reported. A 5 μL of Nafion solution containing graphene-supported platinum nanoparticles (GPNs) was added to the GCE's surface; naturally dried to give the GPNs/GCE [86]. Similarly, the authors separately prepared a graphene-modified electrode (Gr/GCE) and platinum version (Pt/GCE) by dropping 5 μL of 0.5% Nafion solution containing the modifier. They revealed that GPNs showed a better electrochemical performance compared with the bare electrodes and others. In another work, a carbon aerogel electrode modified with about 21.35 nm Ag_2SNPs , was successfully prepared via a method known as the simple solid-vapor reaction [87]. The authors

placed an aluminum foil-covered beaker containing 100 ml H₂O, 3 g of sublimated sulfur, carbon aerogel, and silver in an oven at 110°C, varying the deposition time. They reported that the particles' size is smaller relative to a decrease in the deposition time, suggesting that there was a lesser amount of silver to react with sulfur. Time modification in this bottom-to-top synthesis changes the uniformity and average size of the NPs. The best optical properties were observed at the minimum deposition time, 5 seconds, which presents the agglomeration, and electrical conductivity was increased linearly with time. The authors stated that the modified electrodes show good redox reversibility, unlike the bare electrodes. Hassan *et al.* designed nanoparticles-based electrodes for detecting the presence of naproxen (NAP) in pharmaceutical formulations. Surface modification of carbon paste electrode (CPE) was done by drop-casting 20 µL of SWCNTs suspended in 2 mg·L⁻¹ DMF on inverted CPE and left to dry at 25°C for a day before rinsing with deionized water and was used immediately in the electrochemical cell [88].

Youzhi solely prepared AuNPs-modified-reduced graphene oxide (RGO) nanocomposite modified for determining the presence of Cu²⁺ and Hg²⁺. In the experiment, GCE underwent a series of treatments with alumina (0.05 µm), water, and ethanol; and was oven dried. Then, a solution of RGO in deionized water was ultrasonically dispersed uniformly on the electrode forming a mixed stable solution. Later, 8 µL of the prepared AuNPs-modified-RGO was microinjected on the treated GCE surface and dried at room temperature to give AuNPs-modified-RGO/GCE [89]. The synergistic effect of AuNPs/RGO coupled with large surface area and excellent electrocatalytic activity of the modified electrode ensure its favorable performance as a working electrode in Cu²⁺ and Hg²⁺ sensitive electrochemical sensors. Xinxing's research team designed a gold nanoparticles-modified-carbonized resin nanospheres (AuNPs-modified-CRS-TrGNO) composite with thermally reduced graphene oxide as a scaffold electrode for analysis of Cu²⁺. The matrix-assisted reduction method was adopted for the in-situ synthesis of AuNPs in CRS [90]. This process prevents aggregation and hugely improves the stability of the electrode and its self-redox signal [91] [92]. Consequently, these allow ratiometric electrochemical sensing with high sensitivity, reproducibility, and reliability. The CRS-TrGNO/GCE was modified by immersing it in a solution of 5.0 mM HAuCl₄ and electrodeposited under N₂ atmosphere by a potentiostat method at a potential of -0.2 V and 400 s deposited time. Then, 5 µL of 1% Nafion ethanol solution was spread on the electrode and dried. The AuNPs coated on the carbonized resin nanosphere served as an internal reference probe for the ratiometric determination of Cu²⁺. The components of the resultant electrode all contribute to the increase in the rate of charge transfer, leading to excellent electrochemical performance. Eduart Gutierrez Pineda *et al.* fabricated electrochemical sensors applicable in pharmaceutical, chemical, food industries, and agriculture for detecting and quantifying hydroxylamine and hydrazine. In their work, AuNPs were deposited on polypy-

role/stainless steel (Ppy/SS) electro by dipping the latter in a mixture of 1:5 concentrations of HAuCl_4 and H_2SO_4 . The potential difference of the working electrode was set to 0.8 V for 10 s and then stepped down to -0.8 V for about 1 sec to allow the formation of Au particles on the electrode, and finally increased to 0.1 V for 1 min for particle growth of Au to occur. They called this process a double-step potentiostat routine. The enhanced electrocatalytic behavior, sensitivity, and conductivity of the modified electrodes were reported [18].

4. Characterizations of Nanoparticles Modified Electrodes

Cyclic voltammetry (CV), differential pulse voltammetry (DPV), and electrochemical impedance spectroscopy (EIS) are the three main techniques being used to characterize nanoparticles modified electrodes.

4.1. Cyclic Voltammetry

This assesses the electrochemical properties of material adsorbed on an electrode. In this technique, the potential difference (p.d) of the working electrode changes linearly with time. After a set voltage is reached, the p.d of the electrode potential returns to the initial potential, leading to repeated voltage cycles. The cyclic voltammogram can be measured with the aid of a plot between the working electrode's current (measured between the working and counter electrodes) versus the applied voltage (measured between the working and reference electrode) in respect to time. The rate of voltage change per time during each phase is known as the scan rate of the experiment measured in volts/second (V/s). The cathodic current will increase over the scan rate as the voltage is being applied until the reduction potential of the analyte is reached. The current decreases to signify the depletion of the analyte's (adsorbed substance) concentration. In the case of a reversible electrochemical reaction, an anodic current will arise to indicate the re-oxidation of the reduced analyte at a reverse scan. The more reversible the redox reactions, the more the two sinusoidal peaks look alike.

Common features of CV:

- 1) Redox reaction of electroactive species in solution.
- 2) Electric potential causes adsorption/desorption
- 3) Double layer charging *i.e.* capacitive current
- 4) It can provide a lot of information; so, it is more difficult to analyze.
- 5) Total current density is a sum of both faradaic current and capacitive current

$$j = j_f + j_c \quad (1)$$

where j_f is the faradaic current from the electrode reaction, and j_c is the capacitive current from double-layer charging. Meanwhile, potential changes at a constant sweep rate, *i.e.*

$$v = \frac{dE}{dt} \quad (\text{there is a derivation from the steady state}) \quad (2)$$

$$j = j_f + Cd \frac{dE}{dt} \quad (3)$$

where, $v = \frac{dE}{dt}$.

$$j = j_f + vC_d \quad (4)$$

where v is the double layer correction (it is important when v is large); C_d is the double-layer capacitance.

$$C_d = \frac{\epsilon_o \epsilon_r}{d} A \quad (5)$$

where: ϵ_o is the free space permittivity; ϵ_r is the relative solution permittivity; A is the surface area of the electrode; d is the distance of the Helmholtz layer [93].

Peak occurrence is a result of the interplay of mass transport and diffusion:

Let j_{ac} be activation control from kinetics and j_{diff} be diffusion control from mass transfer [94].

$$\frac{1}{j} = \frac{1}{j_{ac}} + \frac{1}{j_{diff}} \quad (6)$$

When $j = j_{diff}$, and $j = j_{ac}$, at maximum time “ t ”.

That is current increases with electric potential E and time t . j_{ac} and j_{diff} maintain an inverse relationship until the two become approximately equal at a maximum time, t .

But, when $j_{ac} \gg j_{diff}$, current decreases with E and t , so that the Nernst condition can be satisfied, leading to:

$$\Delta E_p = E_{\frac{1}{2}} \pm 2.3026 \frac{RT}{nF} \log \frac{[ox]}{[red]} \quad (7)$$

(peak potential: Nernst equation; and Anodic/cathodic sweep: \pm), where E_p (rev) is the difference between anodic and cathodic peak potentials, and $E_{\frac{1}{2}}$ is the half-wave potential at which $j = \frac{j_{diff}}{2}$. Usually, reversibility is dependent on both v and concentration.

At the cathodic region, the oxidation current is consumed near the electrode, while the reduction current is enhanced near the electrode, given $j \approx 0$ (according to the Nernst equation). The peak is reached at $j = j_p$, $E = E_p$, where reduction current is consumed, and the oxidation current is produced [95].

In continuation to the work of Youzhi, the CV responses to the different electrodes to the same concentration of Cu^{2+} and Hg^{2+} in 0.1 ABS solution at $100 \text{ mV}\cdot\text{S}^{-1}$, are given in **Figure 2**. The curves of bare GCE and RGO/GCE show no significant redox peaks, inferring that the two ions cannot be simultaneously determined. In contrast, the AuNPs-modified-RGO/GCE gave well-defined redox peaks at -0.0655 mV , $+0.0036 \text{ mV}$ (Cu^{2+}), and $+0.261 \text{ mV}$ (Hg^{2+}), suggesting that CV peaks of the said ions can be separated. Moreover, the active area of the modified electrode increased from 0.2232 cm^2 for the bare GCE to 0.4014 cm^2 ,

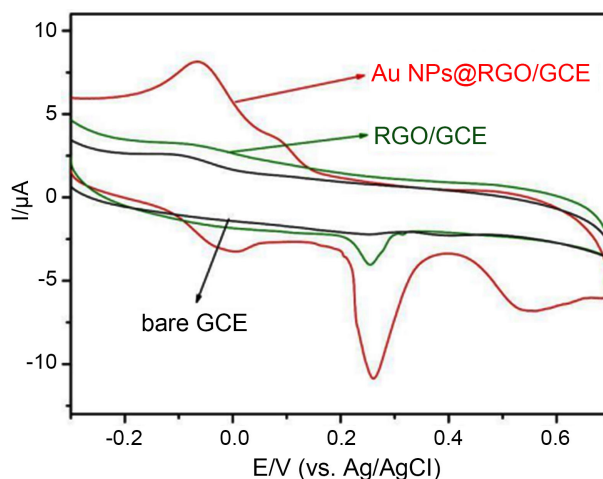


Figure 2. CV of different electrodes in 0.1 M ABS (pH = 5.0) at $100 \text{ mV}\cdot\text{s}^{-1}$.

resulting in the better electrocatalytic activity of AuNPs-modified-RGO/GCE than RGO/GCE or the native electrode for detecting the ions.

In a study, the researchers characterized modified electrodes in a solution of 0.1 M KCl containing 1.0 mM $[\text{Fe}(\text{CN})_6]^{3-/4-}$ complex at a scan rate of 50 mV/s [89]. As shown in **Figure 3**, the poor electrical conductivity of the resin nanospheres (RS) results in a drastic fall in the response current of the complex on the RS modified glass carbon electrode (RS/GCE) compared to the well-defined redox peak observed in the unmodified GCE. In contrast, an increase in the electrochemical response of the complex on AuNPs-modified-RS/GCE was observed due to the good electrochemical activity and high conductivity of AuNPs. An additional increase in the electrochemical response observed when RS was substituted for CRS suggests that the latter has an improved electrical conductivity than RS. Furthermore, the large rectangular area of AuNPs-modified-CRS/GCE indicates its large electrical double-layer capacitance, which is associated with the high conductivity of CRS and the distinct porous structure of carbon [92]. The rectangular area and electrochemical response are higher in the gold nanoparticles-modified-carbonized resin nanospheres composite with thermally reduced graphene oxide as support AuNPs-modified-CRS-TrGNO/GCE. These enhanced properties can be attributed to the large specific surface area, large capacitance, and high conductivity of TrGNO [96]. They gave the CV plot for the above electrodes in 0.6 M NaCl solution as according to **Figure 4**. Here, significantly low redox peaks are observed for the bare GCE and RS/GCE, while an increased redox peak was observed AuNPs@RS/GCE with oxidation and reduction potential peaks at 0.8 V and 0.3 V, respectively. In comparison, higher peak current and finer peak shape are observed at the redox peaks of AuNPs@CRS-TrGNO/GCE. However, the higher intensity and decreased peak difference in the latter shows the faster and easier charge transfer possibility at the electrode surface.

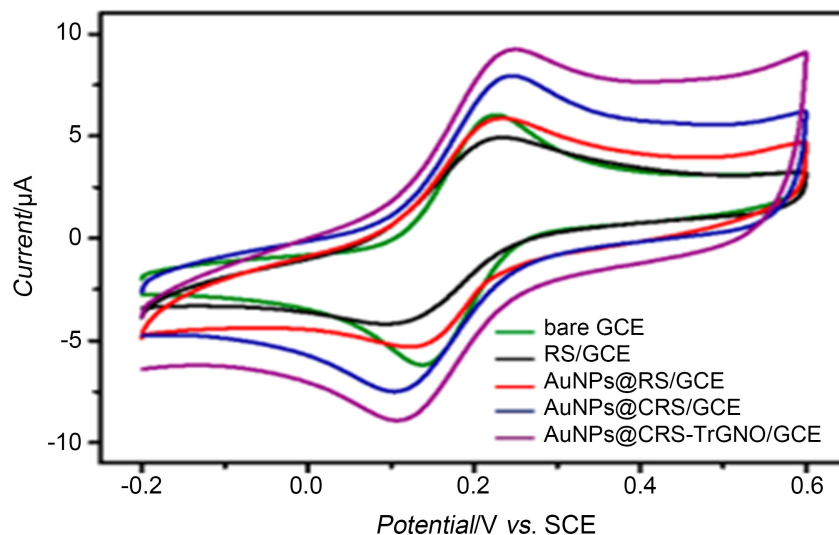


Figure 3. CV plots of native GCE and the modified electrodes in 0.1 M KCl containing electrodes in 0.1 mM $[\text{Fe}(\text{CN})_6]^{3-/4-}$ at $50 \text{ mV}\cdot\text{S}^{-1}$.

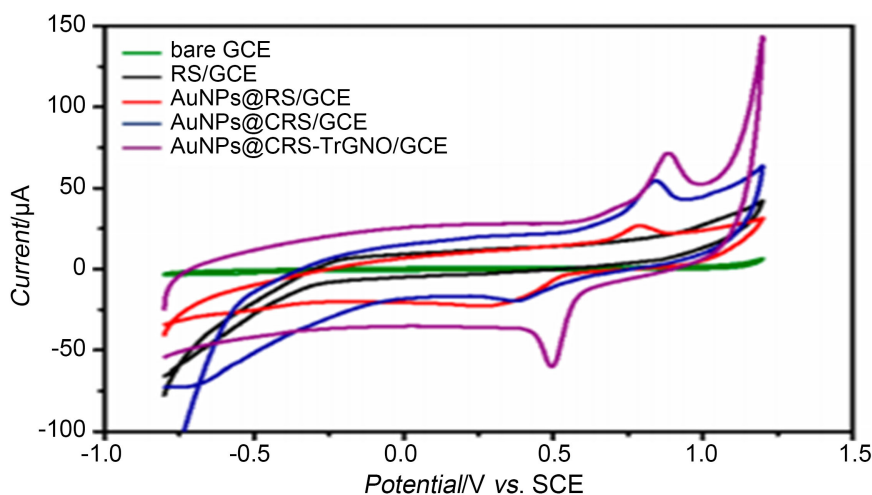


Figure 4. CV plots of native GCE and the modified electrodes in 0.6 M NaCl.

Said and co-workers determined the electrochemical properties of modified pencil graphite electrodes (PGE) using $1 \text{ mM } [\text{Fe}(\text{CN})_6]^{3-}$ as the electrolyte at a scan rate of $100 \text{ mV}\cdot\text{s}^{-1}$. The peak separation, ΔE_p , which represents the rate of electron transfer is significantly large with a broad peak in the bare PGE as shown in **Figure 5**. The ΔE_p becomes smaller on modifying with γ or ϵ - MnO_2 NPs. The electrocatalytic activity was hugely enhanced upon modifying chitosan/PGE with MnO_2 NPs. Here, the separation of the peaks for the cathodic and anodic peaks for the two types of MnO_2 /chitosan-modified PGE was only slightly higher than the theoretical value ($\Delta E_p = 0.059$) signifying the redox couple reversibility of these electrodes, while others demonstrate quasi-reversible behavior at higher values of ΔE_p . The chitosan acts to bind the MnO_2 NPs on the electrode surface leading to an increase in peak current because of the electrocatalytic synergy between them [97].

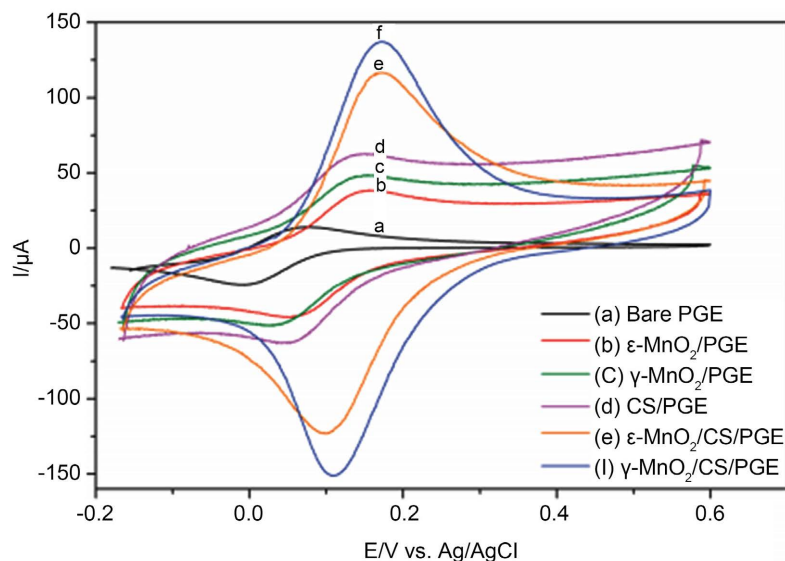


Figure 5. CV of electrodes in 0.1 M KCl containing 1.0 mM $k_3[Fe(CN)_6]$.

Also, Yang *et al.* gave the CV plot of GPNs/GCE using 5 mM $[Fe(CN)_6]^{4-}$ in PBS with 0.1 mol/L KCl. The peak separation of 0.1 V at 100 mV/S associated with GPNs/GCE (**Figure 6**) reveals the redox behavior of $[Fe(CN)_6]^{4-}$. GPNs/GCE shows better electrochemical conductivity compared to other electrodes as supported by its highest peak current, which is twice that of Gr/GCE. With that said, GPNs/GCE was chosen as the best electrode for the enzymatic lactic acid biosensor, giving an excellent performance [85].

Bracamonte and co-workers designed electrochemical sensors for detecting dopamine (DA). CV plots show a small oxidation peak at +0.2 V for the bare carbon paste electrode (CPE), while a strong oxidation and reduction peak around +0.2 V and +0.3 V, respectively, were observed for the nanoceria modified CPE (**Figure 7**). An increase in DA concentration increased the anodic peak current, confirming a redox peak current that arises from the surface-confined DA [82].

Jing Li *et al.* tested the electrochemical behavior of silver nanoparticles/Molybdenum sulfide/reduced graphene oxide modified GCE (AgNPs/MoS₂/rGO) for detecting cardiac troponin 1 using a 5.0 mmol·L⁻¹ $[Fe(CN)_6]^{3-/4-}$ a solution containing 0.1 M KCl [98]. **Figure 8** shows an increase in the redox peak current of the modified GCE because of the electron transfer efficiency and excellent conductivity of RGO. The excellent electrochemical properties of AgNPs and the large surface area of MoS₂ provide an increase in current on modifying the electrode.

Agyapong *et al.* conducted the CV measurements of modified screen-printed carbon electrode (for simultaneous detection of protein and temperature) in 2.5 mM potassium salts of $[Fe(CN)_6]^{3-/4-}$. The features of the native and modified electrodes are shown in **Figure 9**. As expected, there is no distinct paired peak for the unmodified electrode, which depicts that it has a temperature-resistance surface. The peak was almost doubled on modifying with thermochromic. Moreso, TM-AuNPs modified SPCE was more than triple the bare electrodes. For

the AuNPs-modified electrode, the peak current was amplified by six-folds, improving the redox peak; hence, the biological sensitivity [99].

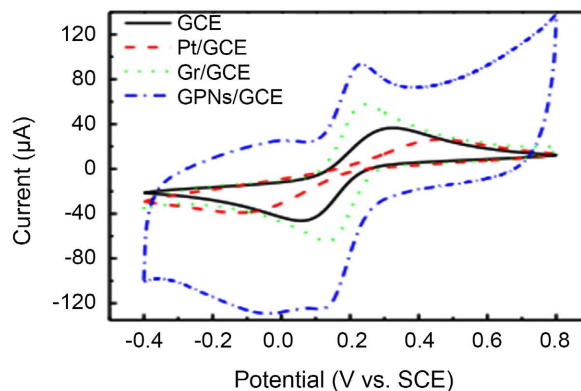


Figure 6. CV of electrodes in 5 mM $[\text{Fe}(\text{CN})_6]^{4-}$ solution at $100 \text{ mV}\cdot\text{S}^{-1}$.

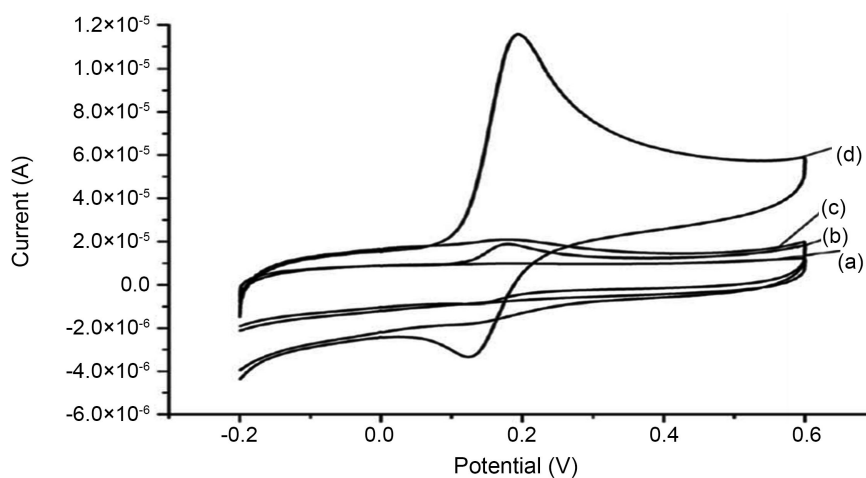


Figure 7. CV of: (a) unmodified CPE, (b) CPE + DA, (c) CPE/nanoceria, and (d) CPE/nanoceria + DA.

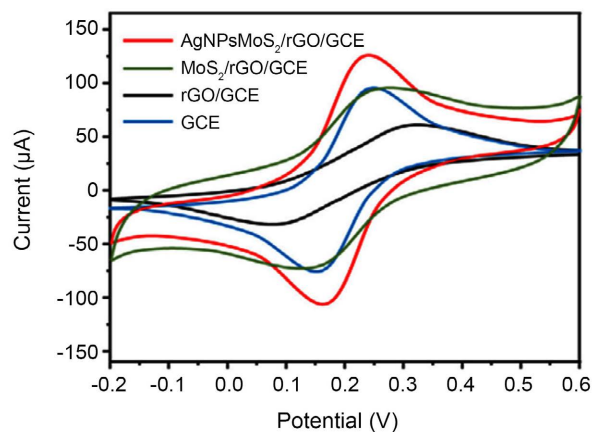


Figure 8. CV plots of $\text{AgNPs}/\text{MoS}_2/\text{rGO}/\text{GCE}$, $\text{MoS}_2/\text{rGO}/\text{GCE}$, rGO/GCE , and bare GCE in 5.0 mM $[\text{Fe}(\text{CN})_6]^{3-/4-}$ at a scan rate of $50 \text{ mV}/\text{S}$.

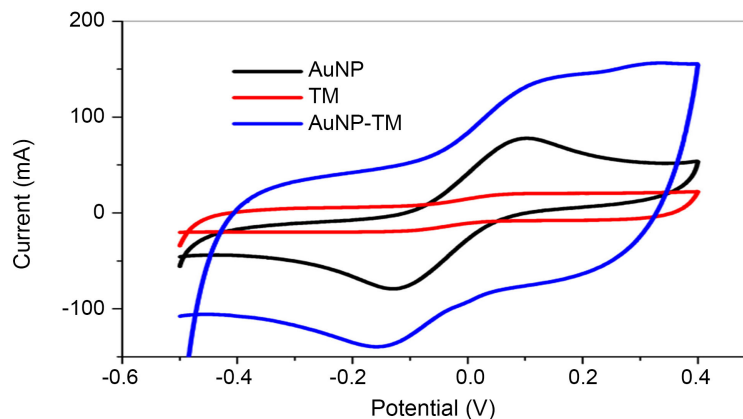


Figure 9. CV plots of 0.0004 mM Hb solution of AuNPs modified SPCE (black); TM modified (red); AuNPs-TM modified (blue).

4.2. Electrochemical Impedance Spectroscopy (EIS)

EIS is a method for measuring the electrical response of a chemical system by applying a range of frequencies at low alternating current (AC) voltages. It is used to determine the electrical and dielectric properties of components in batteries and sensors. Like in CV, three electrodes are used: a working electrode which is the sample material, a reference electrode, and a counter electrode (commonly graphite and platinum). EIS data are often represented on the Nyquist plot or Bode plot. Here, the vertical axis is imaginary data whereas the horizontal axis is the real impedance data. The interpretation is that the plot near the origin represents the solution resistance, whilst the diameter of the curve equals the polarization resistance. In short, EIS translates chemical responses to an interpretable electronic mode being utilized in research such as in semiconductors, batteries, sensors, among others.

EIS is a non-destructive and high information content technique. It is easy to run with a very powerful modeling analysis. It may take up to several hours steps to run analysis. Measurements are made by:

- 1) Applying a small sinusoidal change in potential or current at a fixed frequency.
- 2) Measuring the response at the frequency and doing the same for each other frequency.
- 3) Repeating for a wide range of frequencies, plot and analyze.

EIS modeling:

Usually, complex systems require complex models. Each element in the electric circuit should correspond to specific activity in the electrochemical cell. Do not simply add elements. Use the best fit model for the data. Common elements used are: resistor (in ohms), capacitor (in Farads), inductor (in henrys), Warburg impedance which is a form of resistance to mass transfer, exhibiting a 45° phase shifts, constant phase element used to model imperfect capacitors, exhibiting an 80° - 90° phase shift, and Kramers-kronig transform (states that the magnitude and phase in a real system are related) can be applied to the EIS data

by comparing the calculated magnitudes and the experimental magnitudes to confirm likely similarity. However, if the two magnitudes do not match, then, chances are that the system is not real (not linear, not stable, and not causal).

Youzhi examined the charge transfer rates of different electrodes in 5.0 mM $[\text{Fe}(\text{CN})_6]^{4-/3-}$ a solution containing 0.1 mol·L⁻¹. **Figure 10** indicates the successful modification of the bare GCE, with the largest impedance for bare GCE and smallest for that of AuNPs. The author explained that the difference is due to two factors: an efficient electronic path formed by RGO between electrodes and electrolytes and good conductivity and enlarged surface area of AuNPs@RGO, leading to an increase in electrons conduction on the electrode's surface, and narrows the impedance of the high performing AuNPs@RGO/GCE [88].

In the work of Said and co-workers, EIS was used to determine the electrochemical response at the interface of both the electrode and solution. The non-destructive technique was performed in 1.0 mM of $\text{K}_3[\text{Fe}(\text{CN})_6]$ in 0.5 M KCl at pH 2.5; 10 mV in the frequency range of 1.0 Hz to 10 kHz. The Nyquist plots (**Figure 11**) of the modified PGE give linear graphs associated with a more diffusion-like behavior of the different types of MnO_2 NPs, while a linear plot with a circular path is observed for the bare PGE and CS/PGE. This implies that the presence or absence of MnO_2 NPs plays an important role in the charge transfer process. On top of this, unmodified electrodes show a slow electron transfer rate by giving a circular plot because of the electrodes' high resistivity compared to the modified electrode [97].

In the research conducted by Wang *et al.* on ratiometric electrochemical sensing for detecting copper ions, the authors applied 0.2 V at a high and low frequency of 10⁵ Hz and 0.1 Hz, respectively: maintaining an amplitude of 0.005 V. The Nyquist plots are composed of straight lines and semicircular curve at low and high-frequency regions, respectively. As can be seen in **Figure 12**, the plot of the RS/GCE shows a large semicircular arc (charge transfer resistance)

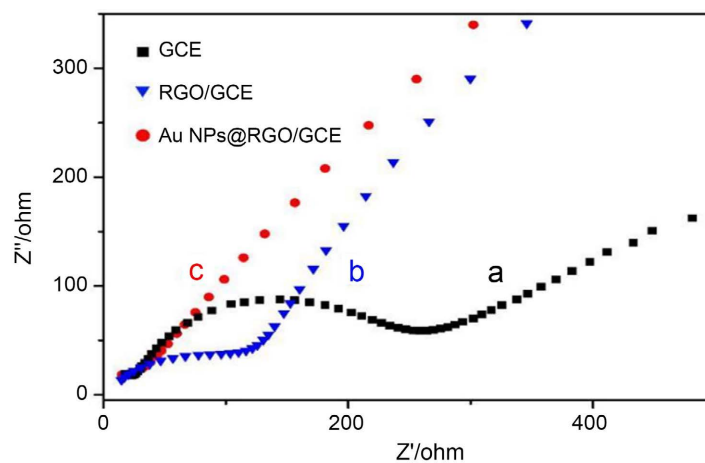


Figure 10. Nyquist plots of EIS of: bare GCE (black), RGO/GCE (blue), AuNPs-modified-RGO/GCE (red) in 5.0 mM $[\text{Fe}(\text{CN})_6]^{4-/3-}$ solution in 0.1 M KCl.

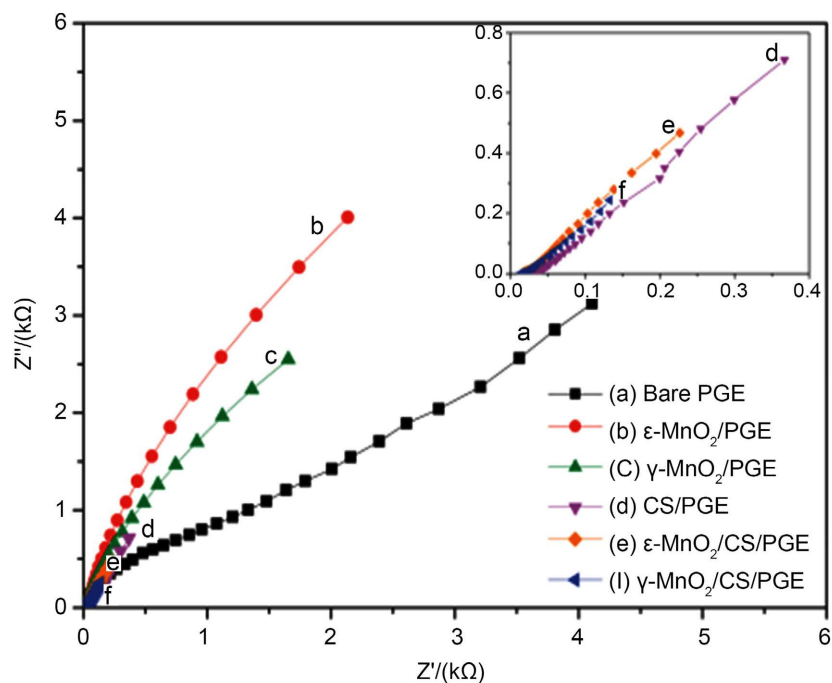


Figure 11. Nyquist plots of EIS measurement of electrodes in 1.0 mM $K_3[Fe(CN)_6]$ in 0.5 M KCl. The inset is a close-up view for (d) CS/PGE; (e) ϵ -MnO₂/CS/PGE; and (f) γ -MnO₂/CS/PGE.

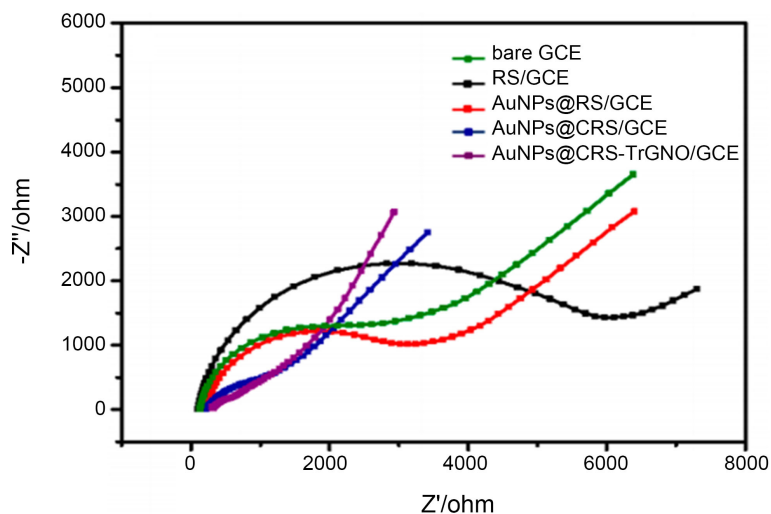


Figure 12. Nyquist plot of native and modified electrodes in 0.1 M KCl containing 1.0 mM $[Fe(CN)_6]^{3-/4-}$.

between the solution and electrode surface, compared with that of unmodified GCE. The higher charge transfer resistivity of RS/GCE is due to the poor conductivity of RS. The arc gradually decreases for AuNPs-modified-RS/GCE, AuNPs-modified-CRS/GCE, and AuNPs-modified CRS-TrGNO/GCE. With the TrGNO-hybridized electrode, the semicircular arc is nearly invisible, which suggests that its higher electrical conductivity compared with others. The AuNPs-modified-CRS-TrGNO/GCE gives lines with a higher slope in the

low-frequency region and about 45° deviation from the classical Warburg diffusion line, indicating its highest diffusion rate among the five electrodes [100].

Similarly, Tang *et al.* gave the Nyquist plots (Figure 13) of EIS measurements obtained from both the bare CPE and ZnO nanorods CPE (Z-CPE) in 0.1 mM citric acid buffer at pH 6.0 with phosphate solution. A big and small semicircle arc in low and high-frequency regions, respectively, indicates an improved charge transfer on the Z-CPE's surface. The citric acid reduced its charge transfer resistivity by modifying the electrode with the ZnO nanorod. They infer that the ZnO nanorods act as a catalyst for electro-oxidation of the citric acid on the electrode surface [101]. Comparatively, the first semicircle is due to the bulk resistance (R_1) that is parallel to the constant phase element (C_1) which creates pathways across the carbon electrode [102]. The second half-circle is attributed to the charge transfer resistance (R_2), parallel to the other constant phase element (C_2) being a characteristic of the double-layer structure formed at the boundary of solution and electrode, whilst R_s is the electrolyte's resistance [103].

Furthermore, Jing *et al.* provided the EIS measurements of the modified electrode. As shown in Figure 14, native GCE presents a small semicircle with the value of electron transfer resistance (R_{ct}) equals 266 Ω . However, the synergistic effects of AgNPs, RGO, and MoS_2 caused the ohmic value to drop to 91 Ω , indicating the enhanced electron transfer effect.

4.3. Differential Pulse Voltammetry (DPV)

It is a method used to measure the redox properties of materials by measuring the current at each point before a successive change in potential. In this technique, the p.d between the reference electrode and the working electrode is being pulsed for about 100 milliseconds from its initial value to an interval potential; then, it changes to a final potential different from the initial potential. The difference in the current before and after the pulse is plotted against the potential. The advantages of DPV include high sensitivity due to the charging current and more precise electrochemical analysis. Its unique features are symmetric and asymmetric peaks for reversible and irreversible reactions, respectively; a detection limit of about 10^{-8} M, and a linear relationship between the concentration and the peak current.

In furtherance of the research of Tang *et al.*, DPV was investigated for the said electrodes by successively injecting 0.5 mM of the electrolyte in 0.1 mol/L phosphate buffer solution (PBS) at pH 6.0 to determine the effect of concentration on the Z-CPE. As shown in Figure 15, the increase in citric acid concentration caused an increase in the current of the electro-catalytic peak at +1.0 V. Hence, there is a proportional relationship between peak current and electrolyte concentration from 0.5 mM to 6 mM ($R^2 = 0.9988$). They reported that the linear relationship fails at a concentration of more than 6 mM, suggesting that the saturation of the ZnO nanorods' active site. This range is better than those obtained from other methods [95].

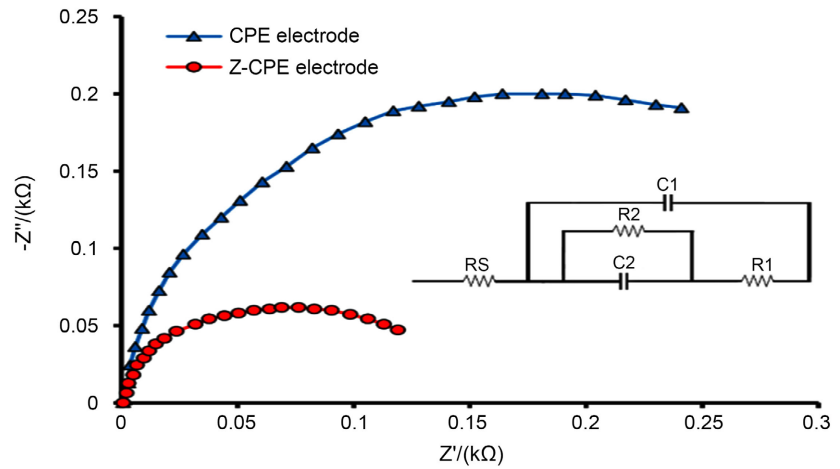


Figure 13. Nyquist plots of EIS analysis from bare CPE and ZnO nanorods CPE. The inset indicates equivalent electrical circuit.

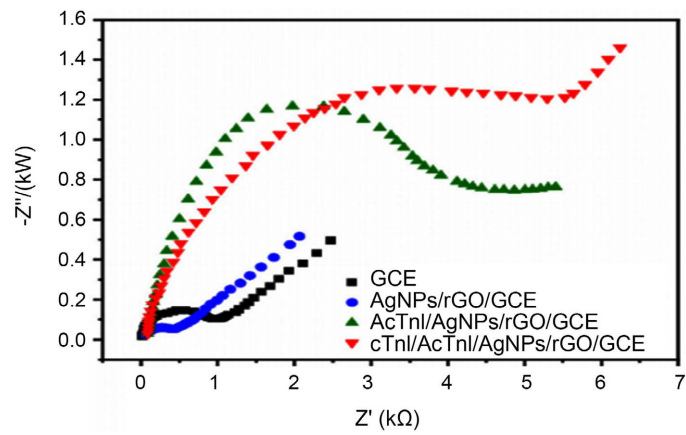


Figure 14. EIS measurements of GCE, rGO/GCE, MoS₂/rGO/GCE and AgNps/MoS₂/rGO/GCE in 5.0 mM [Fe(CN)₆]^{3-/4-}.

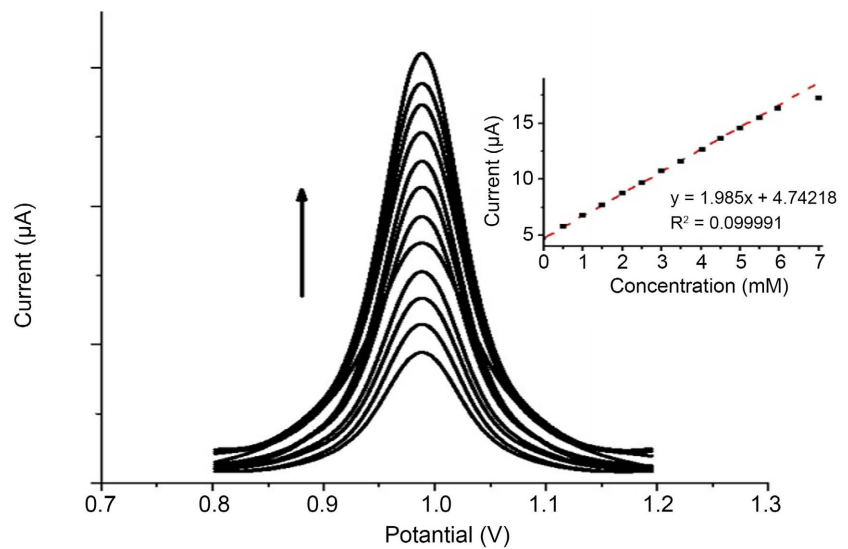


Figure 15. DPV response to Z-CPE to increasing injection of 0.1 μM citric acid in 0.1 M phosphate buffer solution.

Wang *et al.* show the DPV plot (Figure 16) of different compositions of AuNPs-modified CRS-TrGN/GCEs in an electrolyte of 0.6 M NaCl containing 250 $\mu\text{g/L}$ Cu^{2+} . They observed a poor combination of TrGNO with AuNPs@CRS in AuNPs-modified CRS-TrGNO (1:2) due to a low dispersion efficiency, and a slow charge transfer rate in case of the low concentration of TrGNO (0.5 g/L), leaving AuNPs-modified CRS-TrGNO/GCE (1:1) as the most preferable composition. Also, they studied the effect of pH values on the electrochemical response of the electrode.

It is worth knowing as indicated in Figure 16(b) that the peak currents of Cu^{+2} and AuNPs vary inconsistently with different values of pH. While the current intensity of AuNPs reaches its maximum at pH 6, that of Cu^{+2} was pH 5 (0.6 M NaCl) [89]. Moreover, pH 5 was subsequently adopted for the detection because Cu^{2+} was the target of detection.

Sequel to the work carried out by Hassan *et al.*, a comparison was drawn between CV and DPV as applies to the electrochemical behavior of NAP on the native CPE in 0.2 $\text{mol}\cdot\text{L}^{-1}$ PBS at pH 6, 3.0 $\mu\text{g}\cdot\text{L}^{-1}$ and a scan rate of 50 $\text{mV}\cdot\text{S}^{-1}$ [87]. CV gives the anodic peak at 0.999 V corresponding to NAP oxidation, leading to the formation of decarboxylation, and the anodic peak 1.249 V which corresponds

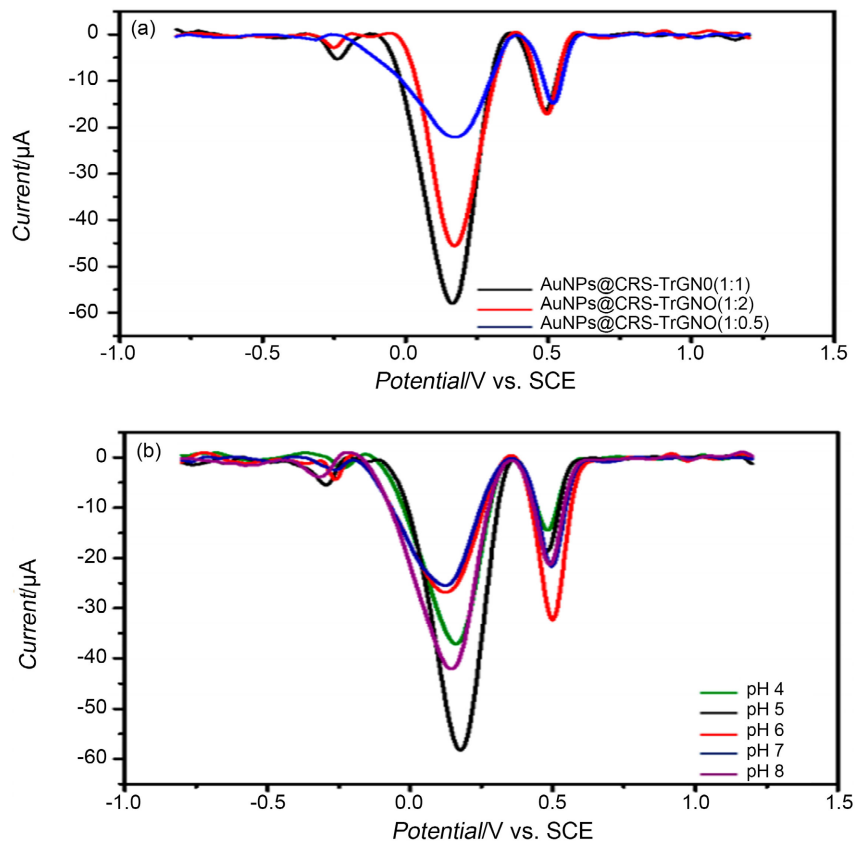


Figure 16. (a) DPV plot obtained from AuNPs@CRS-TrGN/GCEs at different composition ratio in 0.6 M NaCl containing 250 $\mu\text{g/L}$ Cu^{2+} . (b) DPV plot from AuNPs-modified-CRS-TrGN/GCEs in 0.6 M NaCl containing 250 $\mu\text{g}\cdot\text{L}^{-1}$ Cu^{2+} at different pH.

to the current maximum that belongs to 2-acetyl-6-methoxynaphthalene. However, no cathodic peaks were observed suggesting the irreversibility of NAP over the working electrode. In contrast, DPV showed an improved peak height with a sharp and well-defined peak at 0.976 and 1.221 V. Therefore, further quantitative measurements of NAP were carried out using the DPV technique. **Figure 17** also shows the two peaks at 1.06 and 1.25 V associated with the square-wave voltammetry technique but has lower peak height compared with DPV. The latter was recorded using the following parameters: Scan rate, 40 mV/S; pulse time, 40 ms; pulse width 100 ms; pause before the scan, 2 seconds; pulse height, +50 mV. They observed that the CPE became poisoned due to the adsorptive nature of NAP or its oxidation products, leading to a shift in oxidation peaks toward more positive potential and a steady decrease in current on consecutive use of the native electrode. This electrode poisoning was diminished on modifying with SWCNTs, inferring that the latter provides antifouling properties due to faster electron kinetics and no significant shift in the oxidation peaks as shown in **Figure 18**.

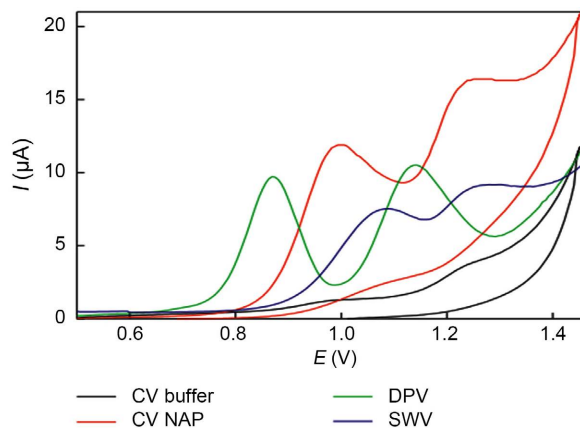


Figure 17. Voltammetric behavior of NAP on the CPE surface in 0.2 M PBS at pH 6.

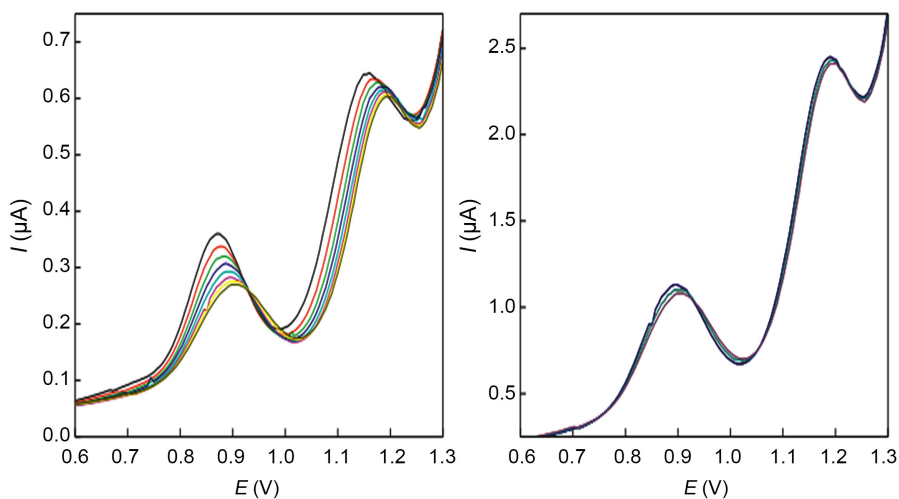


Figure 18. DPV for 8 consecutive measurements of 3 $\mu\text{g}\cdot\text{L}^{-1}$ NAP using (a) CPE, and (b) SWCNTs/CPE, at 50 $\text{mV}\cdot\text{S}^{-1}$.

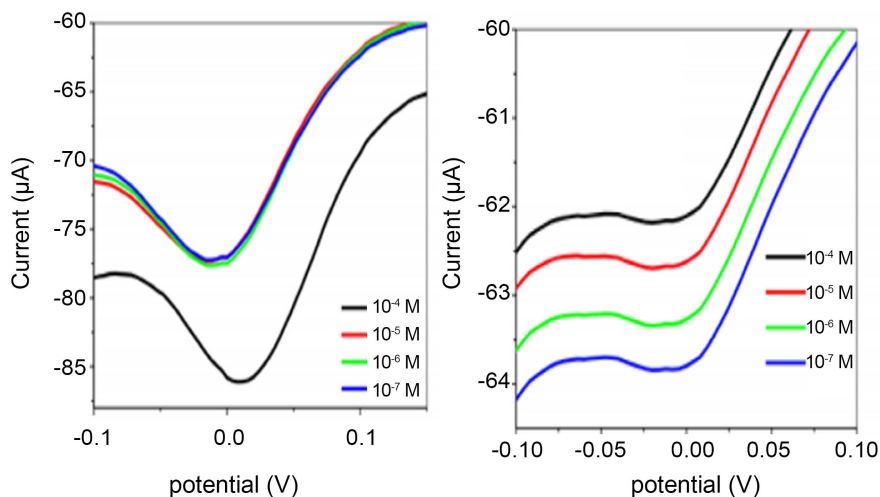


Figure 19. DPV of AuNPs-modified SPCE and TM-AuNPs modified SPCE, respectively.

The DPV measurement reported by Agyapong *et al.* showed an enhanced sensitivity of TM-AuNPs in detecting different concentrations of haemoglobin [C_{Hb}] (Figure 19). At 0 V, a linear relationship existed between the logarithm of the Hb concentration and the peak current from -4 to -7 with a linear fitting equation showing $R^2 = 0.99745$. Overall, the peak current increased as the concentration increases according to the linear equation given as:

$$I_p = -60.398 + 0.581 \log[C_{Hb}].$$

where I_p is the peak current [99].

5. Conclusion and Perspective

Nanoparticles remain highly sought after in modern science due to their large surface area, size distribution, crystallinity, and enhanced electrocatalytic activity. Their methods of synthesis are broadly categorized into two: top-to-bottom and bottom-to-top. The former is toxic, involving several chemical and physical protocols; while the latter is relatively non-toxic, including the green synthesis and chemical reduction. Electrodes modified with nanomaterials have shown improved electrochemical performance compared to bare electrodes, leading to increased sensitivity, lower detection limits, and reproducibility. The enhanced anodic signals of modified electrodes measured by CV and DPV, and more linear rather than circular plots given by EIS are due to the large surface area, more active sites, and high adsorption provided by the nanomaterials.

The gaps in this research area remain to perform both bulk and surface modifications on an electrode with two or more nanoparticles in making it anti-corrosive, then increasing both its lifespan and sensitivity of non-faradaic based miniaturize sensors using nanoparticles to design the capacitor.

The bulk modification involves the incorporation of an additive into the matrix of the electrode. The coating of an electrode surface with two or more nanoparticles has been proven to show better feasibility and effectiveness than us-

ing a sole modifier [104]. Going forward, both modifications can be done on a single electrode. The former would serve to improve the electrochemical response of the working electrode; while the latter, preferable nanomaterials from a metal that is of a lower standard potential and more prone to anodic oxidation than the bulk modifier and the native electrode, would provide cathodic protection, hence, improving the longevity of electrodes.

In addition, there is a need to begin to explore the use of easier to design non-faradaic sensors. The non-faradaic process does not necessitate the use of redox couples, direct current, and a reference electrode, making it possible to be miniaturized—a huge advantage for real-time applications. However, non-faradaic sensors have low sensitivity due to the nature of the charge carriers and their local concentration in the interface of the transducer and substrate. Nanoparticles can come to the rescue due to their high surface area and temperature-stable dielectric which make them capable of handling higher current by storing it. Therefore, when the capacitance of the capacitor (which is the faradaic sensors represented in the Helmholtz layer equation 5 above) increases, the permittivity and subsequent detection capacity of the electrode/sensor will increase. Therefore, designing much more miniaturized non-faradaic sensors should be pivotal in subsequent research in this field.

Acknowledgements

I acknowledge my research advisor Dr. Christopher, Hamaker for his guidance during the articulation of this paper, my friend Ogunlalu Oluwafemi (Ph.D. candidate at the Purdue University, Indiana) for his enlightenment, and fellow master's degree candidates at the Illinois state university Ehlbeck, Josie and Riley Mckenzie for their technical support in this paper and the previous one, respectively.

Conflicts of Interest

The author declares no conflicts of interest regarding the publication of this paper.

References

- [1] Oluwasina, O.O., Akinyele, B.P, Olusegun, S.J., Oluwasina, O.O. and Mohallem, N.D.S. (2021) Evaluation of the Effects of additives on the Properties of Starch-Based Bioplastic Film. *SN Applied Sciences*, **3**, Article No. 421. <https://doi.org/10.1007/s42452-021-04433-7>
- [2] Fay, F., Hansen, L., Hectors, S.J.C.G., Sanchez-Gaytan, B.L., Zhao, Y., Tang, J., *et al.* (2017) Investigating the Cellular Specificity in Tumors of a Surface-Converting Nanoparticles by Multimodal Imaging. *Bioconjugate Chemistry*, **28**, 1413-1421. <https://doi.org/10.1021/acs.bioconjchem.7b00086>
- [3] Sergey, Z. and Valentine, A. (2012) Pd₂(dba)₃ as a Precursor of Soluble Metal Complexes and Nanoparticles: Determination of Palladium Active Species for Catalysis and Synthesis. *Organometallics*, **31**, 2302-2309.

- <https://doi.org/10.1021/om201217r>
- [4] Wei, Q., Xiong, F., Tan, S., Huang, L., Lan, E.H., Dunn, B. and Mai, L. (2017) Porous One-Dimensional Nanomaterials: Design, Fabrication, and Applications in Electrochemical Energy Storage. *Advanced Materials*, **29**, Article ID: 1602300. <https://doi.org/10.1002/adma.201602300>
- [5] Li, W., Elzatahry, A., Aldhayan, D. and Zhao, D. (2018) Core-Shell Structured Titanium Dioxide nanomaterials for Solar Energy Utilization. *Chemical Society Reviews*, **47**, 8203-8237. <https://doi.org/10.1039/C8CS00443A>
- [6] Wang, S. (2008) Controlled Synthesis of Dendritic Au@Pt Core-Shell Nanomaterials for Use as an Effective Fuel Cell Electrocatalyst. *Nanotechnology*, **20**, Article ID: 025605. <https://doi.org/10.1088/0957-4484/20/2/025605>
- [7] Hewakuruppu, Y.L., Dombrovsky, L.A., Chen, C., Timchenko, V., Jiang, X., Baek, S. and Taylor, R.A. (2013) Plasmonic “Pump-Probe” Method to Study Semi-Transparent Nanofluids. *Applied Optics*, **52**, Article ID: 604150. <https://doi.org/10.1364/AO.52.006041>
- [8] Hanagata, N. and Morita, H (2015) Calcium Ions Rescue Human Lung Epithelial Cells from the Toxicity of Zinc Oxide Nanoparticles. *The Journal of Toxicological Sciences*, **40**, 625-635. <https://doi.org/10.2131/jts.40.625>
- [9] Cheraghian, G. and Wistuba, M.P. (2020) Ultraviolet Aging Study on Bitumen Modified by a Composite of Clay and Fumed Silica Nanoparticles. *Scientific Reports*, **10**, Article No. 11216. <https://doi.org/10.1038/s41598-020-68007-0>
- [10] Simoes, F.R. and Xavier, M.G. (2017) Electrochemical Sensors. In: Da Róz, A.L., Ferreira, M., Oliveira, O.N., et al., Eds., *Nanoscience and Its Applications: Micro and Nanotechnologies*, William Andrew, Norwich, 155-178. <https://doi.org/10.1016/B978-0-323-49780-0.00006-5>
- [11] Mehta B.R and Reddy Y.J. (2015) Chapter 6—Fire and Gas Detection System. In: Mehta, B.R. and Reddy, Y.J., Eds.), *Industrial Process Automation Systems: Electrochemical Sensors*, Butterworth-Heinemann, Oxford, 217-235. <https://doi.org/10.1016/B978-0-12-800939-0.00005-X>
- [12] Zhan, F., Liao, X., Gao, F., Qiu, W. and Wang, Q. (2017) Electroactive Crown Ester-Cu²⁺ Complex with *in-Situ* Modification at Molecular Beacon Probe Serving as a Facile Electrochemical DNA Biosensor for the Detection of CaMV 35s. *Biosensors and Bioelectronics*, **92**, 589-595. <https://doi.org/10.1016/j.bios.2016.10.055>
- [13] Tricoli, A. and Bo, R. (2020) Nanoparticle-Based Biomedical Sensors. Cluster Beam Deposition of Functional Nanomaterials and Devices. *Frontiers of Nanoscience*, **15**, 247-269. <https://doi.org/10.1016/B978-0-08-102515-4.00009-X>
- [14] Ozsoz, M., Erdem, A., Kerman, K., Ozkan, D., Tugrul, B., Topcuoglu, N., Ekren, H. and Taylan, M. (2003) Electrochemical Genosensor Based on Colloidal Gold Nanoparticles for the Detection of Factor V Leiden Mutation Using Disposable Pencil Graphite Electrodes. *Analytical Chemistry*, **75**, 2181-2187. <https://doi.org/10.1021/ac026212r>
- [15] Kerman, K., Morita, Y., Takamura, Y. and Tamiya, E. (2005) *Escherichia coli* Single-Strand Binding Protein–DNA Interactions on Carbon Nanotube-Modified Electrodes from a Label-Free Electrochemical Hybridization Sensor. *Analytical and Bioanalytical Chemistry*, **381**, 1114-1121. <https://doi.org/10.1007/s00216-004-3007-1>
- [16] Jeong, E.H., Jung, G., Hong, C.A. and Lee, H. (2014) Gold Nanoparticle (AuNP)-Based Drug Delivery and Molecular Imaging for Biomedical Applications. *Archives*

- of Pharmaceutical Research*, **37**, 53-59.
<https://doi.org/10.1007/s12272-013-0273-5>
- [17] Tripathi, K. and Driskell, J.D. (2018) Quantifying Bound and Active Antibodies Conjugated to Gold Nanoparticles: A Comprehensive and Robust Approach to Evaluate Immobilization Chemistry. *ACS Omega*, **3**, 8253-8259.
<https://doi.org/10.1021/acsomega.8b00591>
- [18] Pineda, E.G., Alcaide, F., Rodríguez Presa, M.J., Bolzán, A.E. and Gervasi, C.A. (2015) Electrochemical Preparation and Characterization of Polypyrrole/Stainless Steel Electrodes Decorated with Gold Nanoparticles. *ACS Applied Materials & Interfaces*, **7**, 2677-2687. <https://doi.org/10.1021/am507733b>
- [19] Singh, S., Jain, D.V.S. and Singla, M.L. (2013) One-Step Electrochemical Synthesis of Gold-Nanoparticles Polypyrrole Composite for Application in Catechin Electrochemical Biosensor. *Analytical Methods*, **5**, 1024-1032.
<https://doi.org/10.1039/c2ay26201k>
- [20] Fan, D., Li, N., Ma, H., Li, Y., Hu, L., Du, B., *et al.* (2016) Electrochemical Immunosensor for Detection of Prostate Specific Antigen Based on an Acid Cleavable Linker into MSN-Based Controlled Release System. *Biosensors and Bioelectronics*, **85**, 580-586. <https://doi.org/10.1016/j.bios.2016.05.063>
- [21] Zhou, Y., Uzun, S.D., Watkins, N.J., Li, S., Li, W., Briseno, A.L., Carter, K.R. and Watkins, J.J. (2019) Three-Dimensional CeO₂ Woodpile Nanostructures to Enhance Performance of Enzymatic Glucose Biosensors. *ACS Applied Materials & Interfaces*, **11**, 1821-1828. <https://doi.org/10.1021/acsami.8b16985>
- [22] Cho, I.H., Kim, D.H. and Park, S. (2020) Electrochemical Biosensors: Perspective on Functional Nanomaterials for *on-Site* Analysis. *Biomaterials Research*, **24**, Article No. 6. <https://doi.org/10.1186/s40824-019-0181-y>
- [23] Tortolini, C., Bollella, P., Zumpano, R., Favero, G., Mazzei, F. and Antiochia, R. (2018) Metal Oxide Nanoparticle Based Electrochemical Sensor for Total Antioxidant Capacity (TAC) Detection in Wine Samples. *Biosensors*, **8**, Article No. 108.
<https://doi.org/10.3390/bios8040108>
- [24] Abdel-Raouf, A.M., Abdel-Monem, A.H., Almrazy, A.A., Mohamed, T.F., Nasr, Z.A. and Mohamed, G.F. (2020) Optimization of Highly Sensitive Screen-Printed Electrode Modified with Cerium(IV) Oxide Nanoparticles for Electrochemical Determination of Oxymetazoline Hydrochloride Using Response Surface Methodology. *Journal of the Electrochemical Society*, **167**, Article ID: 047502.
<https://doi.org/10.1149/1945-7111/ab7180>
- [25] Schedin, F., Geim, A.K., Morozov, S.V., Hill, E.W., Blake, P., Katsnelson, M.I. and Novoselov, K.S. (2007) Detection of Individual Gas Molecules Adsorbed on Graphene. *Nature Materials*, **6**, 652-655. <https://doi.org/10.1038/nmat1967>
- [26] Arsat, R., Breedon, M., Shafiei, M., Spizziri, P.G., Gilje, S., Kaner, R.B., Kalantar-zadeh, K. and Wlodarski, W. (2009) Graphene-Like Nanosheets for Surface Acoustic Wave Gas Sensor Applications. *Chemical Physics Letters*, **467**, 344-347.
<https://doi.org/10.1016/j.cplett.2008.11.039>
- [27] Hafiz, S.M., Ritikos, R., Whitcher, T.J., Razib, N.M., Bien, D.C.S., Chanlek, N., Nakajima, H., Saisopa, T., Songsiriritthigul, P., Huang, N.M. and Rahman, S.A. (2014) A Practical Carbon Dioxide Gas Sensor Using Room-Temperature Hydrogen Plasma Reduced Graphene Oxide. *Sensors and Actuators B: Chemical*, **193**, 692-700.
<https://doi.org/10.1016/j.snb.2013.12.017>
- [28] Chatterjee, S.G., Chatterjee, S., Ray, A.K. and Chakraborty, A.K. (2015) Graphene-Metal Oxide Nanohybrids for Toxic Gas Sensor: A Review. *Sensors and Actuators*

- B. Chemical*, **221**, 1170-1181. <https://doi.org/10.1016/j.snb.2015.07.070>
- [29] Zhu, C.X., Liu, M.Y., Li, X.Y., Zhang, X.H. and Chen, J.H. (2018) A New Electrochemical Aptasensor for Sensitive Assay of a Protein Based on the Dual-Signaling Electrochemical Ratiometric Method and DNA Walker Strategy. *Chemical Communications*, **54**, 10359-10362. <https://doi.org/10.1039/C8CC05829F>
- [30] Sharma, G., Kumar, A., Sharma, S., Naushad, M., Dwivedi, R.P., Alothman, Z.A., Mola, G.T. (2017) Novel Development of Nanoparticles to Bimetallic Nanoparticles and Their Composites: A Review. *Journal of King Saud University: Science*, **31**, 257-269. <https://doi.org/10.1016/j.jksus.2017.06.012>
- [31] Tyagi, H., Kushwaha, A., Kumar, A. and Aslam, M. (2016) A Facile pH-Controlled Citrate-Based Reduction Method for Gold Nanoparticle Synthesis at Room Temperature. *Nanoscale Research Letters*, **11**, Article No. 362. <https://doi.org/10.1186/s11671-016-1576-5>
- [32] Jeyaraj, M., Gurunathan, S., Qasim, M., Kang, M.-H. and Kim, J.-H. (2019) A Comprehensive Review on the Synthesis, Characterization, and Biomedical Application of Platinum Nanoparticles. *Nanomaterials*, **9**, 1719. <https://doi.org/10.3390/nano9121719>
- [33] Zhao, P., Li, N. and Astruc, D. (2013) State of the Art in Gold Nanoparticle Synthesis. *Coordination Chemistry Reviews*, **257**, 638-665. <https://doi.org/10.1016/j.ccr.2012.09.002>
- [34] Zobel, M., Neder, R.B. and Kimber, S.A.J. (2015) Universal Solvent Restructuring induced by Colloidal Nanoparticles. *Science*, **347**, 292-294. <https://doi.org/10.1126/science.1261412>
- [35] Liu, Y., Liu, Y., Yan, R., Gao, Y. and Wang, P. (2020) Bimetallic AuCu Nanoparticles Coupled with Multi-Walled Carbon Nanotubes as Ion-to-Electron Transducers in Solid-Contact Potentiometric Sensors. *Electrochimica Acta*, **331**, Article ID: 135370. <https://doi.org/10.1016/j.electacta.2019.135370>
- [36] Hasaan Hussain, M., Abu Bakar, N.F., Najwa Mustapa, A., Low, K.-F., Hidayati Othman, N. and Adam, F. (2020) Synthesis of Various Size Gold Nanoparticles by Chemical Reduction Method with Different Solvent Polarity. *Nanoscale Research Letters*, **15**, Article No. 140. <https://doi.org/10.1186/s11671-020-03370-5>
- [37] Li, L., Zhang, N., He, H., Zhang, G., Song, L. and Qiu, W. (2019) Shape-Controlled Synthesis of Pd Nanocrystals with Exposed {110} Facets and Their Catalytic Applications. *Catalysis Today*, **327**, 28-36. <https://doi.org/10.1016/j.cattod.2018.07.038>
- [38] Hedkvist, O. and Toprak, M. (2015) Synthesis and Characterization of Gold Nanoparticles. Degree Project in Engineering Physics, First-Level SA104X. KTH Division of Functional Materials, Stockholm.
- [39] Li, J. and Lou, Z. (2020) Importance & Applications of Nanotechnology, Vol. 5, Chapter 2. MedDocs Publishers, Reno, 8-15.
- [40] Frimpong, R., Jang, W., Kim, J.-H. and Driskell, J.D. (2021) Rapid Vertical Flow Immunoassay on AuNP Plasmonic Paper for SERS-Based Point of Need Diagnostics. *Talanta*, **223**, Article ID: 121739. <https://doi.org/10.1016/j.talanta.2020.121739>
- [41] Kim, J.U., Cha, S.H., Shin, K., Jho, J.Y. and Lee, J.C. (2004) Preparation of Gold Nanowires and Nanosheets in Bulk Block Copolymer Phases under Mild Conditions. *Advanced Materials*, **16**, 459-464. <https://doi.org/10.1002/adma.200305613>
- [42] Han, L., Liu, C.-M., Dong, S.-L., Du, C.-X., Li, L.-H. and Wei, Y. (2017) Enhanced Conductivity of rGO/Ag NPs Composites for Electrochemical Immunoassay of Prostate-Specific Antigen. *Biosensors and Bioelectronics*, **87**, 466-472. <https://doi.org/10.1016/j.bios.2016.08.004>

- [43] Rhim, J.W. and Kanmani, P. (2015) Synthesis and Characterization of Biopolymer Agar Mediated Gold Nanoparticles. *Materials Letters*, **141**, 114-117. <https://doi.org/10.1016/j.matlet.2014.11.069>
- [44] Jana, N.R., Gearheart, L. and Murphy, C.J. (2001) Seed-Mediated Growth Approach for Shape-Controlled sYnthesis of Spheroidal and Rod-Like Gold Nanoparticles Using a Surfactant Template. *Advanced Materials*, **13**, 1389-1393. [https://doi.org/10.1002/1521-4095\(200109\)13:18<1389::AID-ADMA1389>3.0.CO;2-F](https://doi.org/10.1002/1521-4095(200109)13:18<1389::AID-ADMA1389>3.0.CO;2-F)
- [45] Paul, A., Solis, J.D., Bao, K., Chang, W.S., Nauert, S., Vidgerman, L., *et al.* (2012) Identification of Higher-Order Long-Propagation-Length Surface Plasmon Polari-ton Modes in Chemically Prepared Gold Nanowires. *ACS Nano*, **6**, 8105-8113. <https://doi.org/10.1021/nn3027112>
- [46] Xue, Y. (2017) Carbon Nanotubes for Biomedical Applications. Industrial Applica-tions of Carbon Nanotubes. In: Peng, H., Li, Q. and Chen, T., Eds., *Industrial Ap-plications of Carbon Nanotubes*, Elsevier, Amsterdam, 323-346. <https://doi.org/10.1016/B978-0-323-41481-4.00011-3>
- [47] Azonano (2013) Multi-Walled Carbon Nanotubes: Production, Analysis, and Ap-plication. Azonano.com.
- [48] Cho, I.H., Lee, J., Kim, J., Kang, M.-S., Paik, J.K., Ku, S., *et al.* (2018) Current Tech-nologies of Electrochemical Immunosensors: Perspective on Signal Amplification. *Sensors*, **18**, Article No. 207. <https://doi.org/10.3390/s18010207>
- [49] Pham, V.P., Jang, S.-H., Whang, D. and Choi, J.-Y. (2017) Direct Growth of Gra-phere on Rigid and Flexible Substrates: Progress, Applications, and Challenges. *Chemical Society Reviews*, **46**, 6276-6300. <https://doi.org/10.1039/C7CS00224F>
- [50] Torres, T. (2010) Carbon Nanotubes and Related Structures. In: Guldi, D.M. and Martín, N., Eds., *Synthesis, Characterization, Functionalization and Applications*, Vol. 135. Wiley-VCH, Weinheim, 215-228.
- [51] Harris, P.J.F., Hirsch, A. and Backes, C. (2009) Carbon Nanotubes Science: Synthe-sis, Properties, and Applications. Vol. 102, Cambridge University Press, Germany, 210-230.
- [52] Thakur, N., Manna, P. and Das, J. (2019) Synthesis, and Biomedical Applications of Nanoceria, a Redox Active Nanoparticle. *Journal of Nanobiotechnology*, **17**, Article No. 84. <https://doi.org/10.1186/s12951-019-0516-9>
- [53] Nadimpalli, N.K.V., Bandyopadhyaya, R. and Runkana, V. (2018) Thermodynamic Analysis of Hydrothermal Synthesis of Nanoparticles. *Fluid Phase Equilibria*, **456**, 33-45. <https://doi.org/10.1016/j.fluid.2017.10.002>
- [54] Junais, P.M. and Govindaraj, G. (2019) Conduction and Dielectric Relaxations in PVA/PVP Hydrogel Synthesized Cerium Oxide. *Materials Research Express*, **6**, Ar-ticle ID: 045914. <https://doi.org/10.1088/2053-1591/aaff14>
- [55] Stelmachowski, P., Ciura, K., Indyka, P. and Kotarba, A. (2017) Facile Synthesis of Ordered CeO₂ NANOROD Assemblies: Morphology and Reactivity. *Materials Che-mistry and Physics*, **201**, 139-146. <https://doi.org/10.1016/j.matchemphys.2017.08.038>
- [56] Fisher, T.J., Zhou, Y., Wu, T.-S., Wang, M., Soo, Y.-L. and Cheung, C.L. (2019) Structure-Activity Relationship of Nanostructured Ceria for the Catalytic Genera-tion of Hydroxyl Radicals. *Nanoscale*, **11**, 4552-4561. <https://doi.org/10.1039/C8NR09393H>
- [57] Jayakumar, G., Albert Irudayaraj, A. and Dhayal Raj, A. (2019) A Comprehensive Investigation on the Properties of Nanostructured Cerium Oxide. *Optical and*

- Quantum Electronics*, **51**, Article No. 312.
<https://doi.org/10.1007/s11082-019-2029-z>
- [58] Khairy, M., Mahmoud, B.G. and Banks, C.E. (2018) Simultaneous Determination of Codeine and Its Co-Formulated Drugs Acetaminophen and Caffeine by Utilizing Cerium Oxide Nanoparticles Modified Screen-Printed Electrode. *Sensors and Actuators, B: Chemical*, **259**, 142-154. <https://doi.org/10.1016/j.snb.2017.12.054>
- [59] Pang, J.-H., Liu, Y., Li, J. and Yang, X.-J. (2019) Solvothermal Synthesis of Nano-CeO₂ Aggregates and Its Application as a High-Efficient Arsenic Adsorbent. *Rare Metals*, **38**, 73-80. <https://doi.org/10.1007/s12598-018-1072-4>
- [60] Sharmila, G., Muthukumar, C., Saraswathi, H., Sangeetha, E., Soundarya, S. and Kumar, N.M. (2019) Green Synthesis, Characterization and Biological Activities of Nanoceria. *Ceramics International*, **45**, 12382-12386. <https://doi.org/10.1016/j.ceramint.2019.03.164>
- [61] Nourmohammadi, E., Kazemi Oskuee, R., Hasanzadeh, L., Mohajeri, M., Hashemzadeh, A., Rezayi, M. and Darroudi, M. (2018) Cytotoxic Activity of Greener Synthesis of Cerium Oxide Nanoparticles Using Carrageenan towards a WEHI 164 Cancer Cell Line. *Ceramics International*, **44**, 19570-19575. <https://doi.org/10.1016/j.ceramint.2018.07.201>
- [62] Proctor, J.E., Armada, D.M. and Vijayaraghavan, A. (2017) An Introduction to Graphene and Carbon Nanotubes. CRC Press, Boca Raton. <https://doi.org/10.1201/9781315368191>
- [63] Bolotin, K.I., Sikes, K.J., Jiang, Z., Klima, M., Fudenberg, G., Hone, J., Kim, P. and Stormer, H.L. (2008) Ultrahigh Electron Mobility in Suspended Graphene. *Solid State Communications*, **146**, 351-355. <https://doi.org/10.1016/j.ssc.2008.02.024>
- [64] Somani, P.R., Somani, S.P. and Umeno, M. (2006) Planar Nano-Graphenes from Camphor by CVD. *Chemical Physics Letters*, **430**, 56-59. <https://doi.org/10.1016/j.cplett.2006.06.081>
- [65] Sun, Z., Yan, Z., Yao, J., Beitler, E., Zhu, Y. and Tour, J.M. (2010) Growth of Graphene from Solid Carbon Sources. *Nature*, **468**, 549-552. <https://doi.org/10.1038/nature09579>
- [66] Guermoune, A., Chari, T., Popescu, F., Sabri, S.S., Guillemette, J., Skulason, H.S., Szkopek, T. and Sij, M. (2011) Chemical Vapor Deposition Synthesis of Graphene on Copper with Methanol, Ethanol, and Propanol Precursors. *Carbon*, **49**, 4204-4210. <https://doi.org/10.1016/j.carbon.2011.05.054>
- [67] Dhand, C., Dwivedi, N., Loh, X.J, Ying, A., Verma, N., Beuerman, R.W., Lakshminarayanan, R. and Ramakrishna, S. (2015) Methods, and Strategies for the Synthesis of Diverse Nanoparticles and Their Applications: A Comprehensive Overview. *RSC Advances*, **5**, 105003-105037. <https://doi.org/10.1039/C5RA19388E>
- [68] Maicu, M., Schmittgens, R., Hecker, D., Glob, D., Frach, P. and Gerlach, G. (2014) Synthesis and Deposition of Metal Nanoparticles by Gas Condensation Process. *Journal of Vacuum Science & Technology A*, **32**, Article ID: 02B113. <https://doi.org/10.1116/1.4859260>
- [69] Tao, A.R., Habas, S. and Yang, P. (2008) Shape Control of Colloidal Metal Nanocrystals. *Small*, **4**, 310-325. <https://doi.org/10.1002/sml.200701295>
- [70] Leong, G.J., Schulze, M.C., Strand, M.B, Maloney, D., Frisco, S.L., Dinh, H.N., Pivovarov, B. and Richards, R.M. (2014) Shape-Directed Platinum Nanoparticle Synthesis: Nanoscale Design of Novel Catalysts. *Applied Organometallic Chemistry*, **28**, 1-17. <https://doi.org/10.1002/aoc.3048>
- [71] Riddin, T., Gericke, M. and Whiteley, C.G. (2010) Biological Synthesis of Platinum

- Nanoparticles: Effect of Initial Metal Concentration. *Enzyme and Microbial Technology*, **46**, 501-505. <https://doi.org/10.1016/j.enzmictec.2010.02.006>
- [72] Martins, M., Mourato, C., Sanches, S., Noronha, J.P., Crespo, M.T.B. and Pereira, I.A.C. (2017) Biogenic Platinum, and Palladium Nanoparticles as New Catalysts for the Removal of Pharmaceutical Compounds. *Water Research*, **108**, 160-168. <https://doi.org/10.1016/j.watres.2016.10.071>
- [73] Gaidhani, S.V., Yeshvekar, R.K., Shedbalkar, U.U., Bellare, J.H. and Chopade, B.A. (2014) Bio-Reduction of Hexachloroplatinic Acid to Platinum Nanoparticles Employing *Acinetobacter calcoaceticus*. *Process Biochemistry*, **49**, 2313-2319. <https://doi.org/10.1016/j.procbio.2014.10.002>
- [74] Shen, D.S., Philip, D. and Mathew, J. (2013) Synthesis of Platinum Nanoparticles Using Dried *Anacardium occidentale* Leaf and Its Catalytic and Thermal Applications. *Spectrochimica Acta Part A: Molecular and Biomolecular Spectroscopy*, **114**, 267-271. <https://doi.org/10.1016/j.saa.2013.05.028>
- [75] Dauthal, P. and Mukhopadhyay, M. (2015) Biofabrication, Characterization, and Possible Bio-Reduction Mechanism of Platinum Nanoparticles Mediated by Agro-Industrial Waste and Their Catalytic Activity. *Journal of Industrial and Engineering Chemistry*, **22**, 185-191. <https://doi.org/10.1016/j.jiec.2014.07.009>
- [76] Du, Y., Lim, B.J., Li, B.L., Jiang, Y.S., Sessler, J.L. and Ellington, A.D. (2014) Reagentless, Ratiometric Electrochemical DNA Sensors with Improved Robustness and Reproducibility. *Analytical Chemistry*, **86**, 8010-8016. <https://doi.org/10.1021/ac5025254>
- [77] Tang, Z.X. and Ma, Z.F. (2016) Ratiometric Ultrasensitive Electrochemical Immunosensor Based on Redox Substrate and Immunophore. *Scientific Reports*, **6**, Article No. 35440. <https://doi.org/10.1038/srep35440>
- [78] Yu, L., Cui, X., Li, H., Lu, J., Kanga, Q. and Shen, D. (2019) A Ratiometric Electrochemical Sensor for Multiplex Detection of Cancer Biomarkers Using Bismuth as an Internal Reference and Metal Sulfide Nanoparticles as Signal Tags. *Analyst*, **144**, 4073-4080. <https://doi.org/10.1039/C9AN00775J>
- [79] Wang, J., Lu, J.M., Hocevar, S.B. and Farias, P.A.M. (2000) Bismuth-Coated Carbon Electrodes for Anodic Stripping Voltammetry. *Analytical Chemistry*, **72**, 3218-3222. <https://doi.org/10.1021/ac000108x>
- [80] Wahyuni Hartati, Y., Nur Topkaya, S., Gaffar, S., Bahtia, H.H. and Cetin, A.E. (2021) Synthesis and Characterization of Nanoceria for Electrochemical Sensing applications. *RSC Advances*, **11**, 16216-16235. <https://doi.org/10.1039/D1RA00637A>
- [81] Jiang, L., Xue, Q., Jiao, C., Liu, H., Zhou, Y., Ma, H. and Yang, Q. (2018) A Non-Enzymatic Nanoceria Electrode for Non-Invasive Glucose Monitoring. *Analytical Methods Journal*, **10**, 2151-2159. <https://doi.org/10.1039/C8AY00433A>
- [82] Meng, F., Miao, H., Shi, J., Hu, Z., Li, G. and Ding, Y. (2017) The Synthesis of Carbon/Cerium Oxide Composites Clusters with the Assistance of the Glucaminium-Based Surfactant and Their Electrochemical Performance in the Glucose Monitoring. *Journal of Alloys and Compounds*, **713**, 125-131. <https://doi.org/10.1016/j.jallcom.2017.04.203>
- [83] Bracamonte, M.V., Melchionna, M., Giuliani, A., Nasi, L., Tavagnacco, C., Prato, M. and Fornasiero, P. (2017) H₂O₂ Sensing Enhancement by Mutual Integration of Single Walled Carbon Nanohorns with Metal Oxide Catalysts: The CeO₂ Case. *Sensors and Actuators B: Chemical*, **239**, 923-932. <https://doi.org/10.1016/j.snb.2016.08.112>

- [84] Huang, H. and Zhu, J.-J. (2019) The Electrochemical Applications of Rare Earth-Based Nanomaterials. *Analyst*, **144**, 6789-6811. <https://doi.org/10.1039/C9AN01562K>
- [85] Iranmanesh, T., Foroughi, M.M., Jahani, S., Shahidi Zandi, M. and Hassani Nadiki, H. (2020) Green and Facile Microwave Solvent-Free Synthesis of CeO₂ Nanoparticle-Decorated CNTs as a Quadruplet Electrochemical Platform for Ultrasensitive and Simultaneous Detection of Ascorbic Acid, Dopamine, Uric Acid and Acetaminophen. *Talanta*, **207**, Article ID: 120318. <https://doi.org/10.1016/j.talanta.2019.120318>
- [86] Yang, C., Yu, S., Yang, Q., Wang, Q., Xie, S. and Yang, H. (2018) Graphene Supported Platinum Nanoparticles Modified Electrode and Its Enzymatic Biosensing for Lactic Acid. *Journal of the Electrochemical Society*, **165**, B665-B668. <https://doi.org/10.1149/2.0341814jes>
- [87] García Martínez, R.R., Rodríguez González, C.A., Hernández-Paza, J.F., Jiménez Vegab, F., Camacho Montesa, H. and Olivás Armendáriz, I. (2021) Synthesis and Characterization of Carbon Aerogels Electrodes Modified by Ag₂S Nanoparticles. *Materials Research*, **24**, Article ID: e20200387. <https://doi.org/10.1590/1980-5373-mr-2020-0387>
- [88] Hendawy, H.A.M., Salem, W.M., Abd-Elmonem, M.S. and Khaled, E. (2019) Nanomaterial-Based Carbon Paste Electrodes for Voltammetric Determination of Naproxen in Presence of Its Degradation Products. *Journal of Analytical Methods in Chemistry*, **2019**, Article ID: 5381031, 9 p. <https://doi.org/10.1155/2019/5381031>
- [89] Yao, Y. (2019) Facile Synthesis of Au Nanoparticles@Reduced Graphene Oxide Nanocomposition-Modified Electrode for Simultaneous Determination of Copper and Mercury Ions. *International Journal of Electrochemical Science*, **14**, 3844-3855. <https://doi.org/10.20964/2019.04.06>
- [90] Wang, X., Liu, G., Qi, Y., Yuan, Y., Gao, J., Luo, X. and Yang, T. (2019) Embedded Au Nanoparticles-Based Ratiometric Electrochemical Sensing Strategy for Sensitive and Reliable Detection of Copper Ions. *Analytical Chemistry*, **91**, 12006-12013. <https://doi.org/10.1021/acs.analchem.9b02945>
- [91] Khan, M.K. and MacLachlan, M.J. (2015) Polymer and Carbon Spheres with an Embedded Shell of Plasmonic Gold Nanoparticles. *ACS Macro Letters*, **4**, 1351-1355. <https://doi.org/10.1021/acsmacrolett.5b00742>
- [92] Kato, D., Kamata, T., Kato, D., Yanagisawa, H. and Niwa, O. (2016) Au Nanoparticle-Embedded Carbon Films for Electrochemical As³⁺ Detection with High Sensitivity and Stability. *Analytical Chemistry*, **88**, 2944-2951. <https://doi.org/10.1021/acs.analchem.6b00136>
- [93] Yao, L., Wu, Q., Zhang, P.X., Zhang, J.M., Wang, D.R., Li, Y.L., Ren, X.Z., Mi, H.W., Deng, L.B. and Zheng, Z.J. (2018) Scalable 2D Hierarchical Porous Carbon Nanosheets for Flexible Supercapacitors with Ultrahigh Energy Density. *Advanced Materials*, **30**, Article ID: 1706054. <https://doi.org/10.1002/adma.201706054>
- [94] Dorledo de Faria, R.A., Dias Heneine, L.G., Matencio, T. and Messaddeq, Y. (2019) Faradaic and Non-Faradaic Electrochemical Impedance Spectroscopy as Transduction Techniques for Sensing Applications. *International Journal of Biosensors & Bioelectronics*, **5**, 29-31. <https://doi.org/10.15406/ijbsbe.2019.05.00148>
- [95] Brett, C.M.A. and Brett, A.M.O. (1993) *Electrochemistry*. Oxford University Press, Oxford.
- [96] Gileadi, E. (1993) *Electrode Kinetics for Chemists, Chemical Engineers, and Materials Scientists*. VCH Verlagsgesellschaft, Weinheim.

- [97] Said, M.I., Rageh, A.H. and Abdel-Aal, F.A.M. (2018) Fabrication of Novel Electrochemical Sensors Based on Modification with Different Polymorphs of MnO₂ Nanoparticles. Application to Furosemide Analysis in Pharmaceutical and Urine samples. *RSC Advances*, **8**, 18698-18713. <https://doi.org/10.1039/C8RA02978D>
- [98] Li, J., Zhang, S., Zhang, L., Zhang, Y., Zhang, H., Zhang, C., Xuan, X., Wang, M., Zhang, J. and Yuan, Y. (2021) A Novel Graphene-Based Nanomaterial Modified Electrochemical Sensor for the Detection of Cardiac Troponin I. *Frontiers in Chemistry*, **9**, Article ID: 680593. <https://doi.org/10.3389/fchem.2021.680593>
- [99] Agyapong, D.A.Y., Jiang, H.J., Ni, X.J., Wu, J.W. and Zeng, H.J. (2021) Gold Nanoparticles/Thermochromic Composite Film on Screen-Printed Electrodes for Simultaneous Detection of Protein and Temperature. *Journal of Biomaterials and Nanobiotechnology*, **12**, 7-19. <https://doi.org/10.4236/jbnb.2021.122002>
- [100] Wang, H., Feng, H.B. and Li, J.H. (2014) Graphene and Graphene-Like Dichalcogenides in Energy Conversion and Storage. *Small*, **10**, 2165-2181. <https://doi.org/10.1002/smll.201303711>
- [101] Tang, H., Gao, T. and Luo, Z. (2020) An Electrochemical Approach for the Determination of the Fruit Juice Freshness Using Carbon Paste Electrode Modified with ZnO Nanorods. *International Journal of Electrochemical Science*, **15**, 2766-2775. <https://doi.org/10.20964/2020.03.37>
- [102] He, X., Deng, F., Shen, T., Yang, L., Chen, D., Luo, J., Luo, X., Min, X. and Wang, F. (2019) Exceptional Adsorption of Arsenic by Zirconium Metal-Organic Framework: Engineering, Exploration, and Mechanism Insight. *Journal of Colloid and Interface Science*, **539**, 223-234. <https://doi.org/10.1016/j.jcis.2018.12.065>
- [103] Naderi, N., Hashim, M., Saron, K. and Rouhi, J. (2013) Enhanced Optical Performance of Electrochemically Etched Porous Silicon Carbide. *Semiconductor Science and Technology*, **28**, Article ID: 025011. <https://doi.org/10.1088/0268-1242/28/2/025011>
- [104] McLamore, E.S., Shi, J., Jaroch, D., Claussen, J.C., Uchida, A., Jiang, Y., Zhang, W., Donkin, S.S., Banks, M.K., Buhman, K.K., Teegarden, D., Rickus, J.L. and Porterfield, D.M. (2011) A Self-Referencing Platinum Nanoparticle Decorated Enzyme-Based Microbiosensor for Real-Time Measurement of Physiological Glucose Transport. *Biosensors and Bioelectronics*, **26**, 2237-2245. <https://doi.org/10.1016/j.bios.2010.09.041>